AD NUMBER

ADB020651

NEW LIMITATION CHANGE

TO

Approved for public release, distribution unlimited

FROM

Distribution authorized to U.S. Gov't. agencies only; Proprietary Info.; Oct 1976. Other requests shall be referred to AFAPL/SFH, Wright-Patterson AFB, OH, 45433.

AUTHORITY

AFWAL ltr, 9 Sep 1983

AD __B020651__

AUTHORITY: _AFWAL_
/try 9 Sep 83
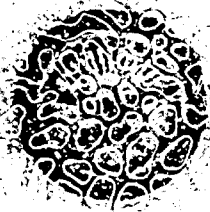
AFAPL-TR-77-11

ADB020651

SOLID ELECTROLYTE OXYGEN SENSOR FOR AIRCRAFT HAZARD PROTECTION APPLICATIONS

UOP INC.

~~CORPORATE RESEARCH~~

TEN UOP PLAZA
DES PLAINES, ILLINOIS 60016

MARCH, 1977

TECHNICAL REPORT AFAPL—TR—77—11
FINAL REPORT FOR PERIOD 26 JANUARY 1976 - 26 NOVEMBER 1976

AD No.
DDC FILE COPY

D D C

AUG 17 1977

AIR FORCE AERO PROPULSION LABORATORY
AIR FORCE WRIGHT AERONAUTICAL LABORATORIES
AIR FORCE SYSTEMS COMMAND
WRIGHT–PATTERSON AIR FORCE BASE, OHIO 45433

This final report was submitted by UOP Inc., under Contract F33615-76-C-2047. The effort was sponsored by the Air Force Aero Propulsion Laboratory, Air Force Systems Command, Wright-Patterson AFB, Ohio under Project 3048, Task 304807, and Work Unit 30480776 with G. T. Beery, AFAPL/SFH as Project Engineer. Dr. L. B. Welsh of UOP Inc. was technically responsible for the work. Other UOP Inc. personnel were: F. R. Szofran, Research Physicist and S. N. Massie, Control Administrator.

Distribution limited to U.S. Government agencies only; Proprietary Info October 1976. Other requests for this document must be referred to Air Force Aero Propulsion Laboratory, WPAFB, Ohio 45433.

This technical report has been reviewed and is approved for publication.

G. T. BEERY
Project Engineer/Scientist

FOR THE COMMANDER

B. P. BOTTERI, Chief
Fire Protection Branch
Fuels and Lubrication Division

REPORT DOCUMENTATION PAGE

READ INSTRUCTIONS
BEFORE COMPLETING FORM

1. REPORT NUMBER	2. GOVT ACCESSION NO.	3. RECIPIENT'S CATALOG NUMBER
AFAPL-TR-77-11		

4. TITLE (and Subtitle)

Solid Electrolyte Oxygen Sensor for Aircraft Hazard Protection Applications.

5. TYPE OF REPORT & PERIOD COVERED

Final Report.
26 Jan 76 - 26 Nov 76,

6. PERFORMING ORG. REPORT NUMBER

7. AUTHOR(s)

L. B. Welsh
F. R. Szofran

8. CONTRACT OR GRANT NUMBER(s)

F33615-76-C-2047

9. PERFORMING ORGANIZATION NAME AND ADDRESS

UOP Inc.
Corporate Research
Ten UOP Plaza
Des Plaines, IL 60016

10. PROGRAM ELEMENT, PROJECT, TASK AREA & WORK UNIT NUMBERS

Project 3048 Task 304807
WU 30480776

11. CONTROLLING OFFICE NAME AND ADDRESS

AFAPL (SFH)
AFWAL
WPAFB OH 45433

12. REPORT DATE

March 1977

13. NUMBER OF PAGES

89

14. MONITORING AGENCY NAME & ADDRESS(if different from Controlling Office)

90 p.

15. SECURITY CLASS. (of this report)

UNCLASSIFIED

15a. DECLASSIFICATION, DOWNGRADING SCHEDULE

16. DISTRIBUTION STATEMENT (of this Report)

Distribution limited to U.S Gov't agencies only; Proprietary Information;
October 1976. Other requests for this document must be referred to
AFAPL/SFH WPAFB OH 45433

17. DISTRIBUTION STATEMENT (of the abstract entered in Block 20, if different from Report)

18. SUPPLEMENTARY NOTES

19. KEY WORDS (Continue on reverse side if necessary and identify by block number)

Oxygen Sensor	rf Sputtering
Fuel Tank Inerting	Solid Electrolyte
Zirconia	
Thin Film	

20. ABSTRACT (Continue on reverse side if necessary and identify by block number)

This program, Solid Electrolyte Oxygen Sensor for Aircraft Hazard
Protection Applications, is concerned with the development of experimental
oxygen sensing devices using this solid electrolyte films. A large number
of these devices have been assembled using this rf-sputter deposited
solid electrolyte films of 8 mole percent yttria-doped zirconia and studied
to determine their physical properties and sensing performance. By varying
the deposition conditions of both the solid electrolyte films and the

DD FORM 1473 EDITION OF 1 NOV 65 IS OBSOLETE
1 JAN 73

electrodes on the films, optimal deposition conditions have been identified. These devices generate an EMF which is quite sensitive to the oxygen partial pressure in the ambient gas.

Various devices have been tested extensively to determine the sensor response time to a change in the oxygen partial pressure, the stability of sensor output, the effect of temperature on the sensing performance, and sensor behavior in the presence of contaminant gases. Response times, for an increase in the oxygen partial pressure of less than one minute are obtained with a typical sensor operated at 150°C. Stable performance over extended periods of time appears to be feasible based on the results of limited lifetime testing. In the presence of contaminant gases, sensor output is altered. In some cases (propane), exposure to the contaminant gas enhances sensor performance. In no case is the sensing performance destroyed by exposure to the contaminants used in this program.

Sensors constructed with optimized electrolyte films and electrodes were subjected to a series of tests designed to simulate aircraft fuel tank ullage space conditions. These results were obtained: (1) Short term exposure to liquid fuel (JP-4) has no deleterious effect on sensor performance but long term exposure may cause an increase in sensor response time. (2) The variation of sensor output at simulated altitudes is in agreement with theory. (3) Temperatures as low as -30°C during device non-operation have neglible effect on sensor performance. (4) Water vapor modifies sensing performance but the sensors continue to operate. (5) Condensation of water onto the sensors alters the performance but does not destroy the sensors. (6) Tank sealant vapors depressed sensor output during sealant curing but oxygen sensing continued in the pre- sence of the vapors. Nearly cured sealant caused relatively smaller alterations in sensor performance.

TABLE OF CONTENTS

TABLE OF CONTENTS (Cont'd)

LIST OF ILLUSTRATIONS

LIST OF ILLUSTRATIONS (Cont'd)

LIST OF TABLES

LIST OF TABLES (Cont'd)

SECTION I

INTRODUCTION AND SUMMARY

1. GENERAL

This document summarizes the results obtained during a two phase program concerned with the initial development, characterization and testing of an aircraft fuel tank ullage space oxygen sensor. This sensor is capable of operating in ambient temperatures below 200°C and uses a thin solid electrolyte film as the sensing element. The technical work under Phase I concentrated on the development of a sensor which would work reliably and predictably under controlled laboratory conditions. In Phase II, sensors fabricated during Phase I were tested in simulated aircraft fuel tank ullage space environments.

Solid electrolytes of the type used in this program have been employed for some time in various high temperature (>400°C) oxygen sensing devices. In these devices the solid electrolyte is generally in the form of a sintered pill or thimble with a characteristic thickness of about 1 mm. Due to the thickness of the solid electrolyte, the response time of these oxygen sensing devices is generally much too long at lower temperatures (<200°C) to meet device requirements. The novel feature of the device under development in this program is that a thin solid electrolyte film (~1 μm), prepared by radio frequency (rf) sputter deposition techniques, is used in place of a thick sintered solid electrolyte pill or thimble to obtain a much faster low temperature response time of the device.

Previous work concerned with this type of sensor was performed under USAF Contract F33615-75-C-2046 by UOP Inc. That work was a feasibility study of four months duration which demonstrated that a device of the type under study could detect changes in the oxygen partial pressure within its environment. Although that program succeeded in proving the feasibility of this type of sensor, sensors developed under that program were neither reliable, reproducible, nor predictable.

During the present contract period the developmental work required to produce a useable oxygen sensing device was initiated. The major objectives of this program were to:

- Prepare thin solid electrolyte films by rf sputter deposition over a range of deposition conditions.

- Characterize the physical and oxygen sensing properties of these films to determine the optimum deposition parameters for films to be used in oxygen sensing devices.

- Assemble sensors with a number of different electrodes to determine the optimum electrode materials and structure.

1

- Characterize the sensor response time dependence on temperature.

- Determine sensor response to selected contaminant gases including a hydrocarbon gas, exhaust gas components, and water vapor.

- Determine sensor performance when exposed to aircraft fuels and tank sealants.

- Determine sensor performance when exposed to reduced pressures and temperatures.

- Determine sensor performance in high humidity environments and following water condensation on the sensor.

2. PROGRAM SCOPE

The complete program covered a period of eleven months. Phase I covered the first nine months. A substantial portion of the Phase I effort was devoted to the determination of rf sputter deposition conditions that would assure reliable thin electrolyte film samples. This required the deposition of many sets of films and the assembly and testing in O_2/N_2 atmospheres of at least a few sensors from each set.

The optimum electrode structure and materials were determined by using the results of resistance measurements of the sensors and additional performance testing of sensors in O_2/N_2 atmospheres.

A substantial portion of the testing of these sensors during Phase I was directed toward a determination of the effect of various contaminant gases on sensor performance. In general, contaminant gases alter the performance of the sensors. To more fully characterize the effects of a contaminant, more tests than those required were performed. The additional testing raised the possibility that the oxygen sensing performance in the presence of fuel vapors may exceed the performance of a sensor in O_2/N_2 atmospheres.

During the Phase II part of this program, those tests which relate to determining the performance of sensors, developed during Phase I, in a fuel tank environment were performed. In addition, five sensors were prepared for delivery to AFAPL/SFH.

The oxygen sensor design and basic concepts on which it is based are presented in Section II. The fabrication of the various parts of the sensor and sensor assembly are detailed in Section III. Test apparatus design and the results obtained during Phase I are presented in Section IV. Section V contains the results of tests performed during Phase II. Conclusions based on test results of Phases I and II are presented in Section VI along with recommendations for future work.

3. PROGRAM ACHIEVEMENTS

The objectives of both Phases I and II have been successfully completed. The most important achievements include:

2

Phase 1

- Preparation of high quality thin solid electrolyte films.

- Demonstrating that dc sputter deposited Pt electrodes produce sensors with much lower internal resistances than any of several other electrode types.

- Assembly of a sensor which produces a repeatable, near theoretical response to changes in oxygen partial pressure in O_2/N_2 atmospheres.

- Sensor response times of less than one minute at temperatures well below 180°C.

- Demonstrating that sensor performance in the presence of contaminant gases is altered but not destroyed and that in the presence of propane, the sensor performance exceeds the performance in uncontaminated O_2/N_2 atmospheres.

Phase II

- Tests to determine sensor performance in a simulated fuel tank environment were successfully completed. Sensors continued to perform as oxygen sensors following all tests.

- Sensors were shown to withstand limited exposure to liquid fuels without degradation of performance.

- Tank sealant vapors were shown to depress sensor output during curing. Relatively smaller alterations in sensor performance were noted with nearly cured tank sealants. For all sensors, oxygen sensing continued in the presence of sealant vapors.

- High humidity and reduced temperature and pressure tests were performed showing that sensors performed as expected based on the Phase I results.

3

SECTION II

OXYGEN SENSOR DESIGN

The design of the thin solid electrolyte film oxygen sensor device is shown schematically in Figure 1. The functions of each element shown in Figure 1 are described below.

1. SUBSTRATE

The substrate provides the mechanical support to prevent destruction of very thin device components. The support can be composed either of electrically insulating or conductive materials. The prime substrate requirement is that it have a very smooth surface free of defects.

2. BACK OR REFERENCE ELECTRODE

In the case of an electrically conductive substrate, the reference electrode and substrate can be identical. For a nonconductive substrate, a metal layer is evaporated onto the substrate. This metal layer serves as the back or reference electrode.

3. SOLID ELECTROLYTE FILM

The solid electrolyte film is rf sputter deposited on top of the reference electrode. A solid electrolyte is a solid material which has a large ionic mobility for one or more of its constituent ions. A thin solid electrolyte film with a high oxygen ion mobility is used in this device to generate an oxygen partial pressure dependent EMF. Between the solid electrolyte film and the reference or back electrode, a metal-metal oxide interfacial region exists which serves to establish a partial oxygen pressure, P_{O_2}'', at the reference electrode.

4. FRONT OR GAS ELECTRODE

On top of the solid electrolyte film, a porous electrode is attached. A high degree of porosity is desired for this electrode to facilitate the adsorption of oxygen gas on the electrode surface, the dissociation of oxygen molecules, and the diffusion of oxygen ions into the solid electrolyte film.

5. LEADS

Electrically conductive leads are attached to the gas and reference electrodes for EMF sensing.

4

SCHEMATIC DIAGRAM OF SENSOR

(E) LEADS

(D) FRONT OR GAS ELECTRODE

(C) SOLID ELECTROLYTE FILM

(B) BACK OR REFERENCE
    ELECTRODE

(A) SUBSTRATE
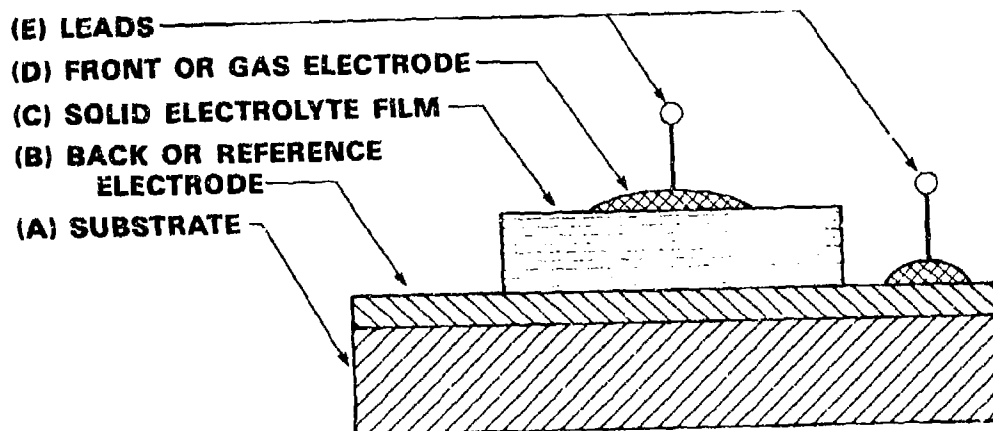
Figure 1 - Schematic Diagram of
Sensor

6. PRINCIPLE OF OPERATION

The EMF generated by a device of the type shown in Figure 1 is dependent on the temperature, the characteristics of the solid electrolyte, and the partial oxygen pressures at the interface of the solid electrolyte with both the gas and reference electrodes. If the partial oxygen pressure at the gas electrode-solid electrolyte film interface, P_{O_2}', is equal to that of the gas itself, then the EMF output of the device is described by the Nernst equation

$$EMF = \frac{RT}{4F} \int_{II}^{I} t_i(P_{O_2}) \, d \ln P_{O_2}. \tag{1}$$

In this equation, the limits of integration are from the reference electrode-solid electrolyte film interface (II) to the gas electrode-solid electrolyte film interface (I). R and F are the gas and Faraday constants, respectively, and T is the absolute temperature. The ionic transference number, $t_i(P_{O_2})$, of the solid electrolyte is defined as the ratio of the ionic conductivity σ_i to the total electrical conductivity or

$$t_i(P_{O_2}) = \frac{\sigma_i}{\sigma_i + \sigma_e} \tag{2}$$

where σ_e is the electronic conductivity. In many instances, the ionic transference number does not depend on the partial oxygen pressure in the solid electrolyte in which case the EMF is given by

$$EMF = \frac{RT}{4F} t_i \ln \frac{P_{O_2}'}{P_{O_2}''} \tag{3}$$

It is important to note the following points:

- The dependence of $t_i(P_{O_2})$ on P_{O_2} depends on the properties of the solid electrolyte film.

- P_{O_2}' and P_{O_2}'' are determined by the properties of the respective interfacial regions.

- P_{O_2}' should correspond to the oxygen partial pressure in the gas.

- The EMF depends logarithmically on P_{O_2}' and linearly on the absolute temperature.

- This equation predicts a 30 mV EMF change when P_{O_2}' is changed from 0.01 to 0.20 atmospheres at 200°C and $t_i = 1$.

- In any gas, P_{O_2}' is defined so that, if P_{O_2}' differs from P_{O_2}'', an EMF will exist.

In the remaining sections of this report P_{O_2} will be used to designate the oxygen partial pressure in the test gas.

FABRICATION OF THE OXYGEN SENSOR DEVICES

In this section the choice of materials and preparative techniques are discussed for the various components of the oxygen sensing device shown schematically in Figure 1.

1. SUBSTRATES AND SUBSTRATE CLEANING

A number of different types of substrates were acquired and studied to determine their usefulness in this program. All substrates were ∿1/2 inch on a side. The relevant features of these substrates are described below.

a. Stainless Steel

Most of the devices tested were fabricated using steel ferrotype substrates. These had a mirror-like finish and were relatively free of defects.

b. Glazed Alumina

Glazed alumina substrates of the type used for electronic microcircuit manufacture were used in the construction of some sensors. Some electrolyte films were deposited on these substrates for analytical purposes such as scanning electron microscope (SEM) fractography analysis of film microstructure.

c. Glass

Microscope cover glasses 0.15 mm nominal thickness were used in the same way as the glazed alumina substrates.

d. Fused Silica

Some films were deposited on these substrates for analytical purposes only. Devices prepared on these substrates would fail because the co-efficient of thermal expansion of fused silica is very small compared to that for either of the solid electrolytes used in this program.

The local surface roughness (peak to peak deviation) of each of the substrates examined is indicated in Table 1. Although the stainless steel substrates are not as smooth as the other types, the electrolyte films adhered better to them and the percentage of successful devices was highest with them.

TABLE 1

SUBSTRATE SURFACE ROUGHNESS

Material	Roughness (nm)
Stainless Steel	356
Glazed Alumina	25
Glass	64
Fused Silica	38

Before deposition of the reference electrode or the solid electrolyte film, all substrates were thoroughly cleaned with organic solvents, mild acid solutions, and by vapor degreasing with trichloroethylene as the final step before loading in the sputtering chamber. The initial steps of the cleaning procedure were changed during the program in order to improve film adhesion. Adhesion is promoted by the removal of all surface dirt but is hindered if the normal oxide layer, in the case of the stainless steel substrates, is removed. At the present time, the cleaning procedure which gives the best results is listed in Table 2.

TABLE 2

SUBSTRATE CLEANING PROCEDURE

Detergent scrub
Deionized water rinse
Methanol wash
Acetone wash
Trichloroethylene wash
Acetone wash
Methanol wash
Deionized water rinse
Etch in solution of 65 g Cr_2O_3, 100 ml H_2SO_4,
   400 ml H_2O at 70°C for 3 minutes
Deionized water rinse
Methanol wash
Acetone wash
Trichloroethylene wash
Trichloroethylene vapor degrease

After cleaning and placing in the sputtering chamber, all substrates are sputter etched. During most of this program this was done for a period of 5 minutes. Toward the end of Phase 1 this time was reduced to avoid possible removal of the oxide layer.

8

2. BACK OR REFERENCE ELECTRODE

In the case of the non-conductive substrates, a metallic Mo layer 0.1 to 0.2 μm thick was deposited by rf sputter deposition. In the case of the metallic substrates, no such layer was necessary.

3. SOLID ELECTROLYTE FILM

As discussed in Section II-3, the solid electrolyte films were prepared by rf sputter deposition. The films were deposited from 4" diameter sputtering targets obtained from Cerac, Inc. Sputtering of these films was performed by Dr. J. Greene at the University of Illinois using a Model 2400 Randex sputtering system. The target to substrate distance was 3.9 cm. Two targets have been used during this program. Most films were deposited with an 8 mole % Y_2O_3/92 mole % ZrO_2 target. The chemical analysis of this target is given in Table 3. The largest impurity concentration listed is hafnium. Since Hf and Zr are isoelectronic, this impurity concentration is not expected to appreciably affect the properties of the sputtered films. In addition to the doped zirconia

TABLE 3

SPECTROGRAPHIC ANALYSIS OF CERAC 8 MOLE %
Y_2O_3/92 MOLE % ZrO_2 SPUTTERING TARGET

Ag	0.001%	Al	0.001%
Ca	0.001	Cu	0.001
Fe	0.01	Mg	0.01
Mo	0.001	Si	0.05
Sn	0.001	Ti	0.01
V	0.001	Hf	Est. 1%

films, five sets of 5 mole % Y_2O_3/95 mole % CeO_2 films were also deposited to determine the influence of sputtering conditions on film microstructure. The analysis of the doped ceria target is shown in Table 4.

TABLE 4

SPECTROGRAPHIC ANALYSIS OF CERAC 5 MOLE %
Y_2O_3/95 MOLE % CeO_2 SPUTTERING TARGET

SiO_2	95 ppm	ThO_2	300 ppm
Fe_2O_3	105	La_2O_3	100
CaO	300	Gd_2O_3	250
Al_2O_3	500	Dy_2O_3	300
MnO_2	100	Er_2O_3	100
MgO	11	Yb_2O_3	40

9

During each rf sputter deposition run, 25 substrates in a 5 x 5 array could be used to obtain as many electrolyte films. The film thickness decreased with distance from the center of the array and the corner films were 63% as thick as the central film in each batch. The relation between substrate position in the holder and normalized film thickness is given in Table 5.

TABLE 5

RELATIVE THICKNESS OF THIN FILMS BY POSITION NUMBER

Film Position[a]	Relative Thickness
1,5,21,25	0.63
2,4,6,10,16,20,22,24	0.75
3,11,15,23	0.83
7,9,17,19	0.89
8,12,14,18	0.94
13	1.00

[a] Film positions are numbered row-wise in a 5 x 5 array.

By altering the rf bias on the substrate, different types of Y_2O_3-doped ZrO_2 films were grown by rf sputter deposition. Those deposition parameters which were varied are listed in Table 6. Other parameters which were not varied include the argon sputtering pressure within the sputtering chamber, P_{Ar} = 20 m Torr, and the target voltage, V_T = -500 V, except as noted. The sputtering system was upgraded between the deposition of the type 6 and type 7 films. This included changes in the vacuum system and caused some changes in the sputtering parameters required to achieve a given quality film. This is characteristic of the practice of rf sputtering and does not alter the qualitative validity of data obtained from the first 6 film types. Specifically, the film microstructure will vary qualitatively in the same way with substrate bias but the exact values of the applied bias voltage will depend on the details of the sputtering system. The sputter run numbers are assigned by the consultant who makes the films. They are not consecutive in all cases but it has been convenient to use them for sensor designation in this program.

The film thickness for a given type of film was determined simply by the length of time during which deposition took place. The deposition rates for the sputtering conditions used for the first six types are shown in Figure 2. Film thickness measurements were made by optical interferometry and with a surface roughness analyzer.

TABLE 6

rf SPUTTER DEPOSITION CONDITIONS, OXYGEN-TO-ZIRCONIUM
ATOMIC RATIOS, FILM THICKNESSES, AND TENTATIVE
CRYSTALLOGRAPHIC ORIENTATIONS FOR Y_2O_3-DOPED ZrO_2 FILMS

Type	V_S[a] (V)	Sputter Run	O/Zr (%)[b]	Thickness[c] (μm)	Orientation[d]
1	0	38	-	0.33	111 or 100
		39[e]	88	0.24	
2	-20	46	-	0.27	111 or 100
		50[e]	90	0.55	111 or 100
3	-40	35	92	2.3	
		36	-	2.9	111
4	-60	41	103	1.0	110
5	-80	42	100	1.2	110
6	-100	40	94	0.61	100
7	-50	102[e]	-	-	110
8	-40	103[e]	-	-	
		105[e]	-	1.3	

[a] Applied substrate bias.

[b] Percent of stoichiometric ratio, 2.26 for 8 mole % Y_2O_3-doped ZrO_2.

[c] At the central film location.

[d] Tentative identification of crystallographic direction(s) normal to the films.

[e] Target voltage = -300 V.

The microstructure of the films varied from columnar at low values of the applied substrate bias V_S to quite uniform at larger values of V_S. This was determined by SEM fracture studies of the films and typical examples are shown in Figure 3. The film grown with V_S = -40 V is characteristic of all films grown with $-V_S \leq 40$ V for film types 1-6 and the film grown at V_S = -80 V characterizes those grown with $-V_S \geq 60$ V. Film types 7 and 8 have not yet been analyzed by this technique.

Auger electron spectroscopy (AES) was used to determine the oxygen to zirconium atomic ratios listed in Table 6. The Y lines were obscured in the AES spectra and x-ray photoemission methods (ESCA) were used to determine that the Y to Zr ratio was the same in the films as in the target.

DEPOSITION RATES FOR DOPED ZIRCONIA
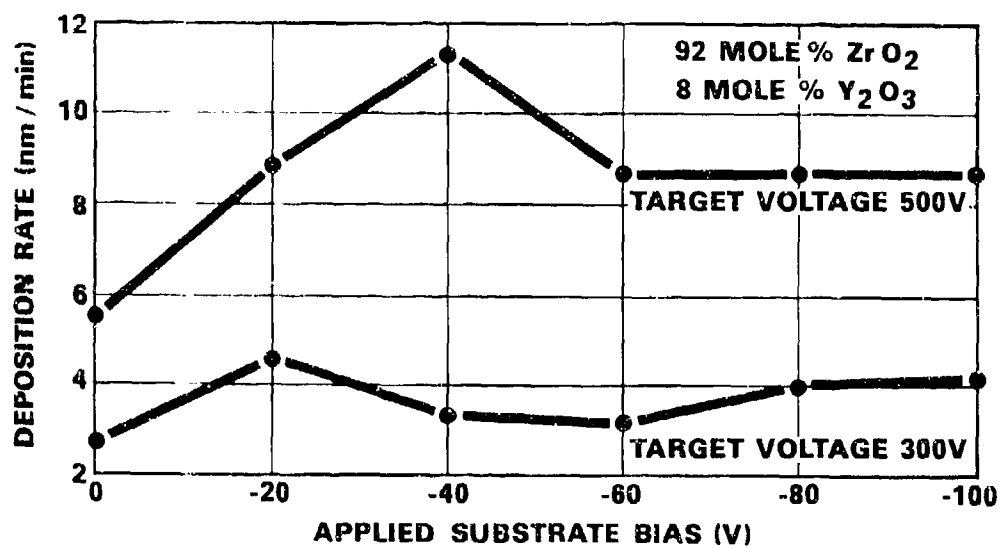
Figure 2 - Deposition Rates for
Doped Zirconia

$V_T = -500 \text{ V}$

$P_{Ar} = 20 \text{ mTorr (2.67 Pa)}$

$V_s = -40 \text{ V}$ (a)

$V_s = -80 \text{ V}$ (b)

1 μm
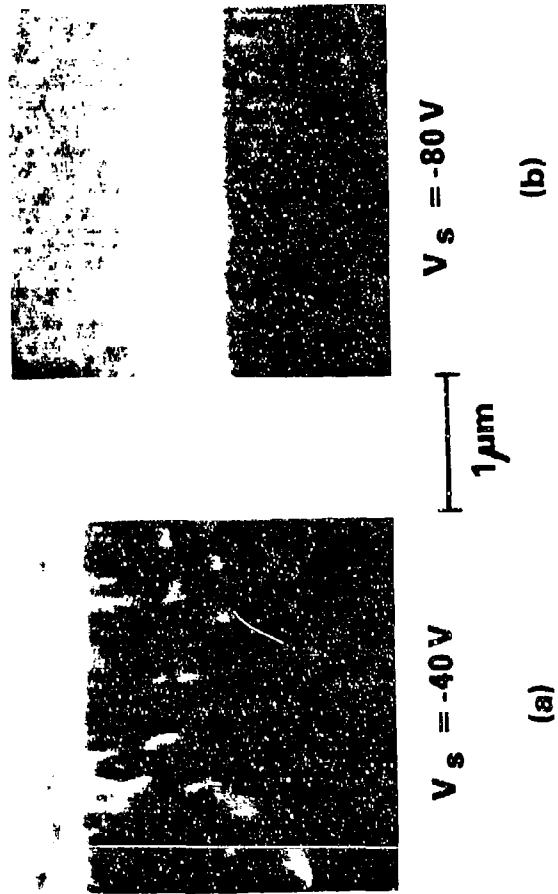
Figure 3 - Doped Zirconia Thin Film Microstructure

A cubic crystal structure was observed for all films examined by x-ray diffraction. A camera specifically designed for thin film work was used. The films exhibited a high degree of preferred orientation and the crystallographically preferred directions were dependent on the applied substrate bias. A tentative identification of the crystal directions perpendicular to the plane of the film is given in Table 6. While the assignments are tentative, the important point is that the films grow in a preferred direction which is dependent on V_S.

Five sets of Y_2O_3-doped CeO_2 films were grown to determine the dependence of the microstructure and atomic structure on V_S. All sets were grown with $V_T = -1000$ V and $P_{Ar} = 20$ mTorr. As in the case of the doped ZrO_2 films, these films were cubic with preferred growth directions dependent on V_S. The microstructure, however, was uniform for $V_S = 0$ and increasingly columnar for increasing magnitudes of V_S. This is opposite to the doped ZrO_2 results and is not understood at this time. Sputter deposition parameters and results are shown in Table 7 and the deposition rates for doped CeO_2 films are shown in Figure 4.

TABLE 7

rf SPUTTER DEPOSITION CONDITIONS, FILM THICKNESSES AND TENTATIVE
CRYSTALLOGRAPHIC ORIENTATIONS FOR Y_2O_3-DOPED CeO_2 FILMS

Type	V_S^a (V)	Sputter Run	Thickness (μm)	Orientation[b]
1	0	9	0.68	110
2	-40	13	0.54	111
3	-80	10	0.60	110 or 111
4	-110	12	0.48	311
5	-140	11	0.33	310

[a] Applied substrate bias.

[b] Tentative identification of crystallographic direction(s) normal to the film.

4. FRONT OR GAS ELECTRODE

Four types of gas electrodes were tested on sensor devices. These electrode types are listed below.

a. dc sputter deposited Pt. The most reliable electrodes used during this program were dc sputter deposited between 30 and 100 nm thick. Tests to be described in Section IV also indicate that sputtered Pt electrodes provide the highest electrode-electrolyte interfacial conductance.

14

DEPOSITION RATES FOR DOPED CERIA

DEPOSITION RATE (nm/min)

95 MOLE % CeO_2
5 MOLE % Y_2O_3

TARGET VOLTAGE 1000V

APPLIED SUBSTRATE BIAS (V)
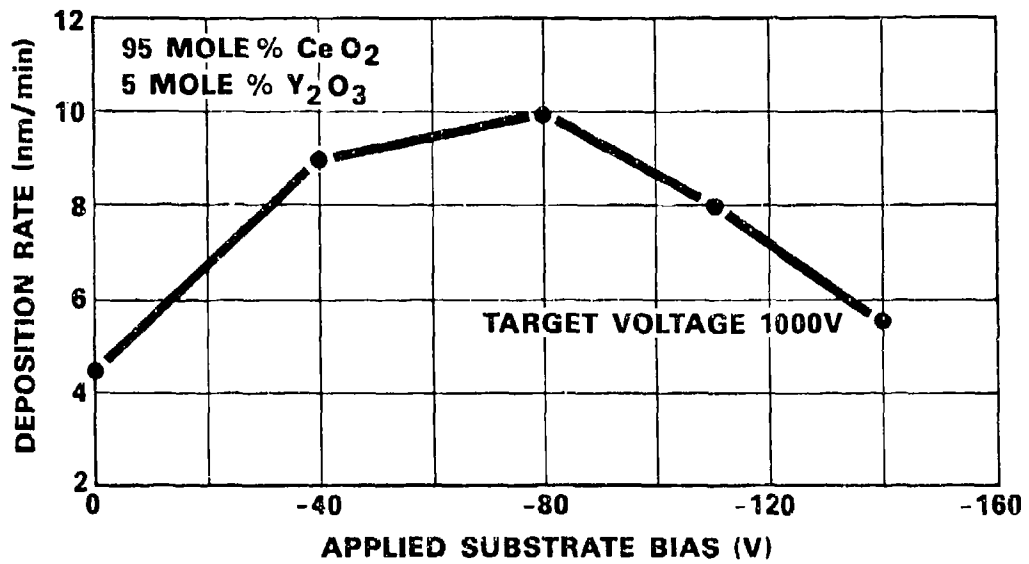
Figure 4 — Deposition Rates for
Doped Ceria

15

b. Pt applied as a colloid. A colloid of Pt particles in an organic vehicle (Electro Materials Corp. of America 4231) was applied directly to the electrolyte film and then dried by heating in air or an O_2/N_2 atmosphere. These electrodes provided good sensors in many cases. However, they were extremely fragile and are not suitable for use outside the laboratory.

c. dc sputter deposited Au. One sensor was tested with a 70 nm thick electrode of this type. It showed generally good sensing characteristics and proved durable but had a much slower response time than sputter deposited Pt electrodes. This single test should not be considered conclusive. Au electrodes may be useful for sensor operation in the presence of certain contaminants.

d. Vapor deposited Ag. These electrodes performed well initially but deteriorated rapidly due to oxidation.

5. LEADS AND LEAD ATTACHMENT

Pt, Au and Cu leads were used in sensor device fabrication. All were 0.010 inch diameter wires. The leads were attached with one of the following:

a. Pt colloid. The same material used for electrodes and described above. This was used with Pt colloid and sputtered Pt electrodes.

b. Au colloid. This material was similar to the Pt colloid and was used with the sputtered Au and some of the sputtered Pt electrodes.

c. Ag colloid. Used with the vapor deposited Ag electrodes only.

d. Pressure contact. This was used successfully with the sputtered Pt and sputtered Au electrodes. (The sensor with the sputtered Au electrode was tested this way initially and later the lead to the gas electrode was attached with the Au colloid.)

No distinction could be made among the lead materials except that Cu could not be used when a pressure contact was made. This was attributed to the oxidation of the Cu surface.

16

The lead attachment techniques used to date have been chosen for convenient sample mounting and demounting in laboratory test apparatus. More durable contacts for prototype sensing devices can be applied using standard microcircuit techniques.

6. DEVICE PACKAGE

Figure 5a shows three doped ZrO_2 films on stainless steel, glazed alumina, and glass substrates. The optical interference fringes resulting from the variation in the film thickness are visible in the photograph which was taken with a colored filter. The horizontal band on the glazed alumina and glass substrates is the Mo back electrode. The first step in integrating the films into a sensor device is the application of a front or gas electrode. The upper part of Figure 5b shows two films on stainless steel substrates with a sputter deposited Pt electrode on the left-hand film and a Pt colloid electrode on the right-hand film.

The lower part of Figure 5b shows a sensor device ready for testing. The film electrode sub-assembly is mounted on a glass cover slide inside the metal can with RTV (room temperature vulcanizing rubber). Two wire leads are placed through the can and insulated by a two-holed ceramic thermocouple insulator. The leads and the insulator are made rigid and sealed with a ceramic cement (Sauerisen No. 31). The leads are then attached to the electrodes using Pt colloid as shown or by one of the other methods discussed previously.

17

Figure 5 - Thin Films and
Sensor Assembly

STAINLESS STEEL SUBSTRATE **GLAZED ALUMINA SUBSTRATE** **GLASS SUBSTRATE**
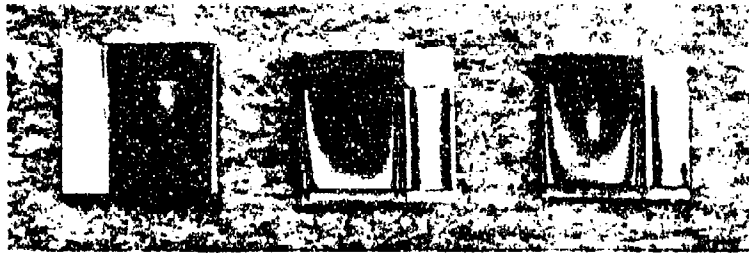
(a)

SPUTTERED PT ELECTRODE

PT PASTE ELECTRODE

ASSEMBLED SENSOR

(b)

18

SECTION IV

OXYGEN SENSOR PERFORMANCE - PHASE 1

1. DEVICE TEST APPARATUS

Two different types of data were recorded for selected sensors:

- The resistance as a function of P_{O_2} and T.

- The EMF dependence on P_{O_2}, T, and contaminant gases.

a. Apparatus for Resistance Measurements

Variations of the sensor resistance with temperature were measured in air using an infrared furnace. The furnace temperature was controlled to within ±1°C and was measured with a thermocouple attached to a digital readout pyrometer. The dependence of sensor resistance on P_{O_2} was measured in the EMF apparatus described in the next section. All resistance data included in this report were taken either with a vector impedance meter (Hewlett-Packard 4800A) in the range 5 Hz to 500 kHz or with an electrometer.

b. Apparatus for EMF Measurements

The apparatus used for the EMF measurements consists of the following systems:

(i)   Gas handling system. An automatically operated eight stream selector valve was used which could be programmed to provide a cycle of two to eight different gas mixtures. Each valve position could be maintained for 1-60 minutes before switching to the next position. The valve position could also be controlled manually. Gas flow rates were measured with rotameters. Most gas mixtures were purchased and used directly from the cylinders. In-house gas mixing was required for several tests. In this case the individual gas flow rates were measured using separate rotameters before the gas lines were combined.

(ii)   Temperature control and measurement system. Sensor testing was normally performed in an oven capable of temperatures exceeding 270°C. A proportional controller with a thermocouple sensor was used to maintain the desired temperature. The temperature was measured with a thermocouple placed inside the sensor test chamber (to be described in the next paragraph). A digital readout pyrometer similar to that used for resistance measurements was used to read the measuring thermocouple. The measured temperature depended somewhat on the gas flow rate but, with a constant flow rate, the temperature was maintained to within ±1°C.

(iii)   Sensor test chambers. Two types of sensor test chambers were used. The first type is shown in Figure 6a and was used for simultaneous testing of up to six sensors. Three sensor assemblies could be

19

Figure 6 - Sensor Test Chambers

**SIX PORT TEST CHAMBER
SHOWING THREE PORTS. SENSORS
ARE MOUNTED ON TWO PORTS**
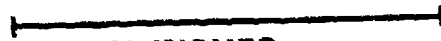
10 INCHES
(a)

RESPONSE TIME TEST CHAMBER

1.5 INCHES
(b)

20
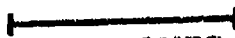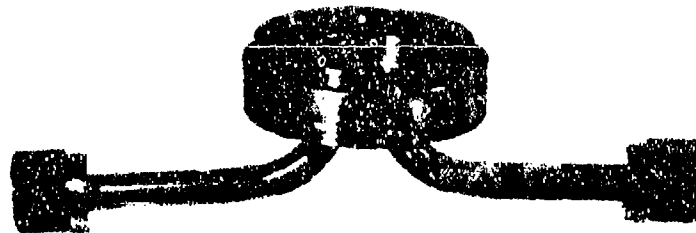
mounted on each side of the chamber. On the side visible in the figure, two sensors are mounted and one port remains open. This type of chamber was used for most testing in Phase 1 of this program but the chamber volume was too large for response time testing. A small volume is required to reduce the flush time so that true sensor response times can be obtained. The test chamber shown in Figure 6b was constructed for this purpose. These chambers could be mounted in series in the oven so that several sensors could be tested simultaneously.

(iv) EMF measuring and recording apparatus. Electrometers with input impedances $\geq 10^{14}$ Ω were used as unity gain, impedance matching amplifiers between the sensors and the multi-pen strip chart recorder used to record the EMF data. The electrometers could also be operated in a mode in which the input impedance could be varied between 10 Ω and 10^{11} Ω in decade steps. This feature was used to determine the apparent internal resistance of several sensors.

2. TEST GAS MIXTURES

The nominal and measured concentrations of gas mixtures used during Phase 1 are shown in Table 8. These gas mixtures were purchased from Matheson Gas Products and were "Certified Standard" grade. The analysis accuracy for each component is ±2%. In each case the balance is N_2.

In addition to the gas mixtures listed in Table 8, a cylinder of chemically pure propane ($\geq 99\%$ purity in the liquid phase) was also used for some tests.

In order to identify which sensing data were obtained using particular gas mixtures, Table 8 also lists the correlation by figure number of data and gas mixtures employed.

TABLE 8

CORRELATION BY FIGURE NUMBER OF SENSING
DATA AND GAS MIXTURES EMPLOYED

Nominal Concentrations		Analysis Results		
Oxygen	Other	Oxygen	Other	Figure(s)
20%		20.34%		15
		20.16		8-14, 19-23
		20.25		16-18, 24, 25, 27
10		10.07		8, 12-15, 19-23
		10.25		16-18, 24, 25, 27
5		4.94		12-15
3		3.15		
		3.16		8, 19-23
		3.08		16-18, 24, 25, 27

21

TABLE 8 (CONT'D)

Nominal Concentrations		Analysis Results		
Oxygen	Other	Oxygen	Other	Figure(s)
1%		1.01%		15[b]
		_[a]		8, 12-14, 15[b], 19-23
		1.07		9, 10, 11
		1.01		16-18, 24-27
3	250 ppm H_2O	3.04	265 ppm H_2O	19
3	10% CO_2	2.69	10.02% CO_2	20
3	0.1% NO_2	2.90	0.098% NO_2	21
3	0.01% SO_2	3.24	0.010% SO_2	22
1	1.5% C_3H_8	1.08	1.52% C_3H_8	23-26

[a] Analysis not supplied by vendor.

[b] Part of the data in Figure 15 were taken with each 1% O_2 mixture indicated.

3. DEVICE RESISTANCE DATA

The resistance of a number of sensors was measured by both ac and dc techniques to determine the temperature and P_{O_2} dependence of the various resistive processes that contribute to the total device resistance. A careful separation of these resistive contributions allows information to be obtained about various electrode processes as well as acting as a method by which the electrolyte film may be characterized and compared with the bulk electrolyte material.

a. Optimization of the Sensor Electrodes

The dc resistance of a sensor device is composed essentially of three parts: (1 and 2) the so-called charge transfer resistance at the interface of the electrolyte with each electrode and (3) the electrolyte resistance. In order to separate these contributions to the total resistance it is not sufficient to measure only the dc resistance of a sensor. The individual contributions can be distinguished under certain conditions by measuring both components (resistive and reactive) of the ac impedance over an appropriate frequency range.

Due to the magnitude of the internal resistance of solid electrolyte sensor devices, it is important to minimize each resistance to the greatest extent commensurate with good sensing characteristics. (Recall that this is the motivation for using thin film instead of bulk electrolytes.) Con-

sequently, the chief electrode optimization goal for this program was to determine the charge transfer resistances of several types of electrodes that might be used as gas electrodes. These electrodes were tested at high temperatures on bulk electrolyte samples. Bulk samples were used for the following reasons:

- The same type of electrode could be applied to either side of the bulk sample. This made the ac impedance data analysis much simpler than if a thin film sample with two different kinds of electrodes had been used.

- A detailed analysis of the electrode portion of the impedance data for thin film samples was often not possible at temperatures much below 550°C.

- Electrode types which could not be applied to current thin film samples but may be useful in production models could be tested. This includes Pt and Au colloids which were used in the thin film sensors without the normal baking step at the high temperatures (~950°C) required to sinter the metals.

The results of these tests are listed in Table 9. The conductance (reciprocal of resistance) per unit area is shown in Siemens/square meter at 552±2°C for seven electrode types. The bulk electrolyte has the same chemical composition as the doped zirconia target used to make films for this program. It is clear that the sputter deposited Pt electrodes are substantially better in terms of their dc resistance than any other type tested. It is also clear that there are variations in resistance with the thickness of the Pt with 70 nm being optimum for the bulk electrolyte. If the electrode resistance is determined by the microscopic coverage of the electrolyte, then the optimum Pt thickness for thin film electrodes is somewhat less than 70 nm. This is because the thin film surface is smoother than the bulk electrolyte surface and it therefore has less microscopic surface area per unit of geometric surface area.

TABLE 9

ELECTRODE CONDUCTANCE

CONDUCTANCE PER UNIT AREA OF ELECTRODES ON 8 MOLE % Y_2O_3–
92 MOLE % ZrO_2 BULK ELECTROLYTE. THE DATA WERE TAKEN
AT OR INTERPOLATED TO 552±2°C.

Electrode Type	Conductance Per Unit Area (S/m^2)
Sputtered Pt, 100 nm thick	63.6
Sputtered Pt, 70 nm thick	156.0
Sputtered Pt, 50 nm thick	131.0
Pt paste	2.6
Pt paste with moderate glass loading	<0.2
Sputtered Au, 70 nm thick	7.0
Au paste	5.0
Ag paste	oxidizes

Based on these results, sputter deposited Pt electrodes were used almost exclusively during the latter part of Phase I and for all Phase II work. Electrodes were generally 50-70 nm thick.

b. Comparison of Thin Film and Bulk Electrolyte Properties - Temperature Dependence

In contrast to the difficulty in determining thin film-electrode interfacial resistances by impedance measurements, the resistance of the thin electrolyte films can be determined at temperatures as low as 150-200°C. The electrolyte resistance of a selected set of sensors has been determined as a function of temperature in air at temperatures up to 550°C. An example of the data obtained is shown in Figure 7, a plot of log (R/T) versus T^{-1} for the electrolyte of sensor no. 50Zr-20. (The number means the film from position 20 in sputter run 50 with the doped ZrO_2 target was used.) A 4.8 mm diameter dc sputter deposited Pt gas electrode 70 nm thick was used for each of the sensors on which electrolyte resistance measurements were made. From the linear relationship between log (R/T) and T^{-1}, some important conclusions can be drawn. First, the film conductivity can be represented by the equation $\sigma = (A/T) \exp (-E_a/kT)$, where A is a constant, k is Boltzmann's constant, and E_a is the temperature independent activation energy for the conduction process. Second, there is a single conduction process over the temperature range of these measurements. These results and the EMF data to be discussed later in this Section indicate that the conductivity in these films is a result of oxygen ion mobility.

The activation energies for several films deposited with applied substrate biases between 0 and -80 V are listed in Table 10. The values are close to the bulk value which has been determined in the same temperature range to be 0.99 eV. The resistance (impedance) measurements were made in order of decreasing temperature so that each sample was essentially heat treated prior to the measurement of its activation energy. Auger electron spectroscopy measurements indicate that heating oxygen deficient films in air causes them to approach stoichiometry so that the differences in O/Zr ratio among the films that were used was reduced by the time the electrical measurements were made. The cause for the discrepancies between bulk and thin film activation energies has not been identified, but possibilities include residual differences in O/Zr ratios and stresses within the films.

24

TEMPERATURE DEPENDENCE OF ELECTROLYTE RESISTANCE
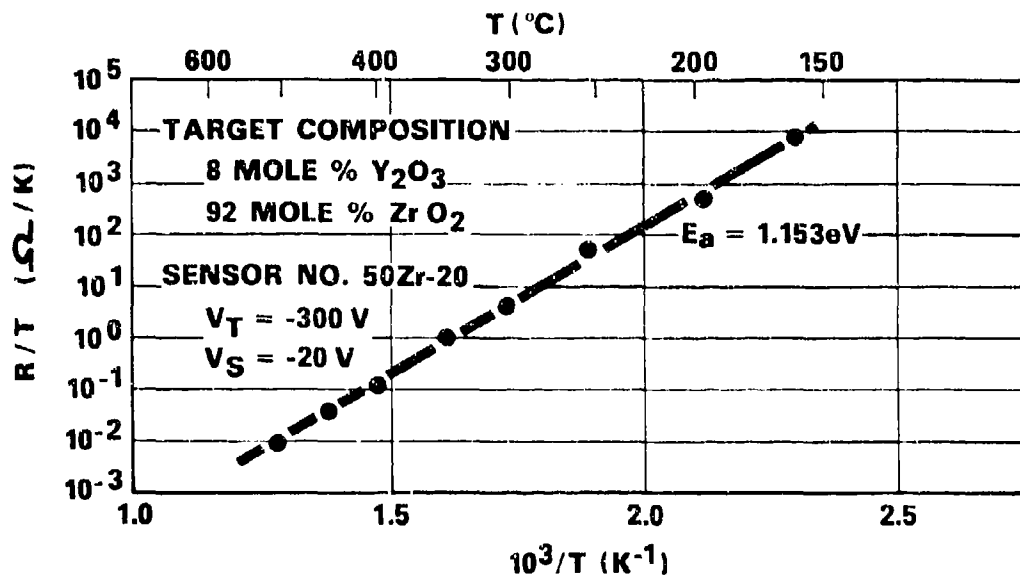
Figure 7 - Temperature Dependence
of Electrolyte Resistance

TABLE 10

CONDUCTIVITY ACTIVATION ENERGIES, RESISTANCE,
AND RESISTIVITY OF SELECTED DOPED ZrO_2 FILMS

Type	V_s^a (V)	E_a^b (eV)	R^d (kΩ)	ρ^d (MΩ-m)
1	0	0.89	33	2.9
2	-20	1.15[c]	174[c]	7.7[c]
3	-40	1.15	-[e]	-[e]
4	-60	1.09	200	3.7
5	-80	1.19	192	3.4

[a]Applied substrate bias.

[b]Oxygen ion conductivity activation energy

[c]$V_T = -300$ V.

[d]Electrolyte resistance R and resistivity ρ at T = 199±3°C.

[e]At 248°C, R = 45 kΩ and $\rho = 0.5$ MΩ-m.

c. Oxygen Partial Pressure Dependence

No measureable dependence of sensor resistance on oxygen partial pressure in the range 0.01 to 0.20 atm was found.

4. DEVICE EMF DATA IN O_2/N_2 ATMOSPHERES - ATMOSPHERIC PRESSURE

a. Test Procedure and Typical Data

The sensing performance of individual sensors was nominally characterized by measuring the EMF response of the sensor to a standard O_2/N_2 gas cycle. The standard gas cycle for this testing was

$$N_2 \rightarrow 1\% \ O_2 \cdot 3\% \ O_2 \rightarrow 10\% \ O_2 \rightarrow 20\% \ O_2 \rightarrow N_2$$
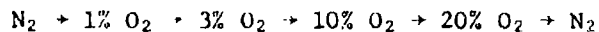
with the balance of all oxygen mixtures being nitrogen. During the first part of the program a 5% O_2 mixture was used instead of the 3% O_2 mixture. Typically 5-20 minutes elapsed between gas mixture changes. An example of the type of data obtained from two sensors that performed moderately well is shown in Figure 8. These data have been photographically reproduced to show the quality of the data. All other EMF data of this type included in this report are tracings of actual data.

PHOTOGRAPH OF O_2/N_2 CYCLE DATA RECORD
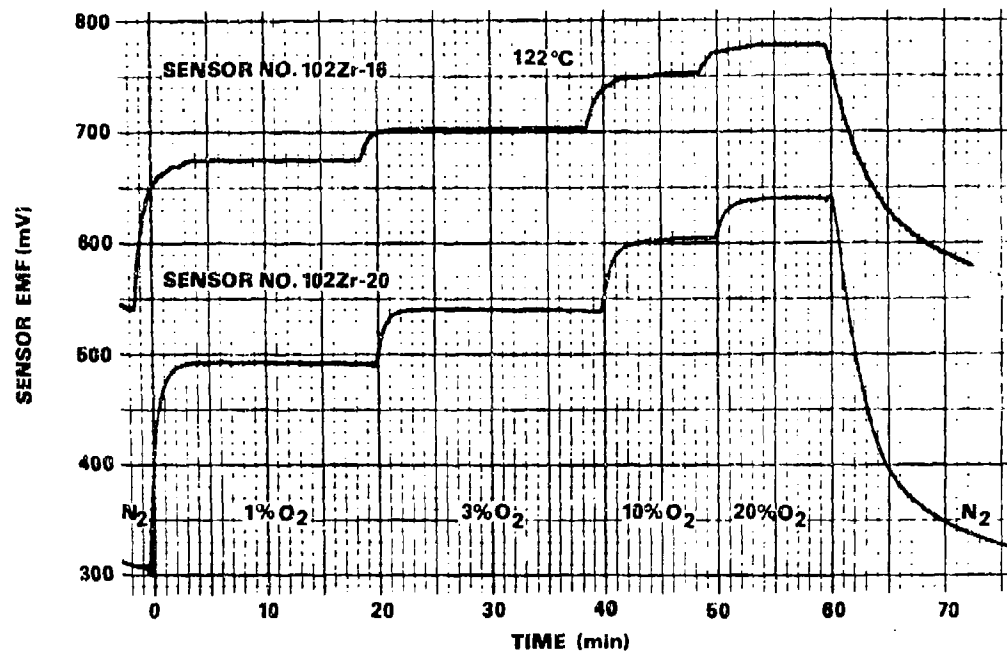
Figure 8 — Photograph of O_2/N_2
Cycle Data Record

The rapidity with which the EMF output of a sensor responds to a change in the oxygen partial pressure was determined by a different procedure. For the response time testing the gas was cycled between the 1% O_2 and 20% O_2 mixtures. The results of these response time tests will be presented next and will be followed by the discussion of the other aspects of sensor response in O_2/N_2 atmospheres.

b. Temperature Dependence of Sensor Response Time

The response time of several sensors with sputter deposited Pt electrodes was measured at five temperatures in the range of 90-180°C. For the purposes of this report, response time is defined as the time required for the change in sensor EMF to reach 90% of the final value. The response time was measured for changes in oxygen partial pressure of both 0.01 to 0.20 atm and 0.20 to 0.01 atm (1% O_2 to 20% O_2 and 20% O_2 to 1% O_2).

Results at several temperatures, taken in order of increasing temperature, are shown in Figure 9 for a typical sensor. These data were taken the first time this sensor was heated. The shorter response time measured for an increasing oxygen concentration than for a decreasing oxygen concentration is shown in this figure and is a general characteristic of sensor response. Similar data for two other sensors have been analyzed and the results are plotted in Figures 10 and 11, respectively. In these two figures, τ_{1-20} and τ_{20-1} are the response times for changes in oxygen concentration from 1% to 20% and from 20% to 1%. The response times are plotted logarithmically against T^{-1} and they fall reasonably well on straight lines. This indicates a response time temperature dependence of the form $\tau = \tau_0 \exp(E/kT)$ where τ_0, k and E are constants. The value of E is indicated for each solid line in Figures 10 and 11. The lines are least squares fits to the data points.

Both of these sensors have response times τ_{1-20} less than one minute for temperatures greater than 160°C. The τ_{20-1} values are larger but the τ_{1-20} values are of more importance for inerting applications.

c. O_2/N_2 Tests – General Results

In the process of testing sensors with different types of electrodes and different types of electrolyte films, scores of sensors were assembled and tested. Some of these were kept under test for periods as long as a month. A tabulation of selected data from a variety of sensors is presented in Table II. This table includes data obtained early in the program with a gas handling system that is suspected of having been contaminated and is presented primarily to indicate that a large number of sensors were tested successfully. In some cases the results are also affected by outgassed contaminants from the RTV used to mount the sensors to the test chamber. Finally, there is substantial evidence that sensors with oxygen deficient electrolyte films produce

RESPONSE TIME TESTS
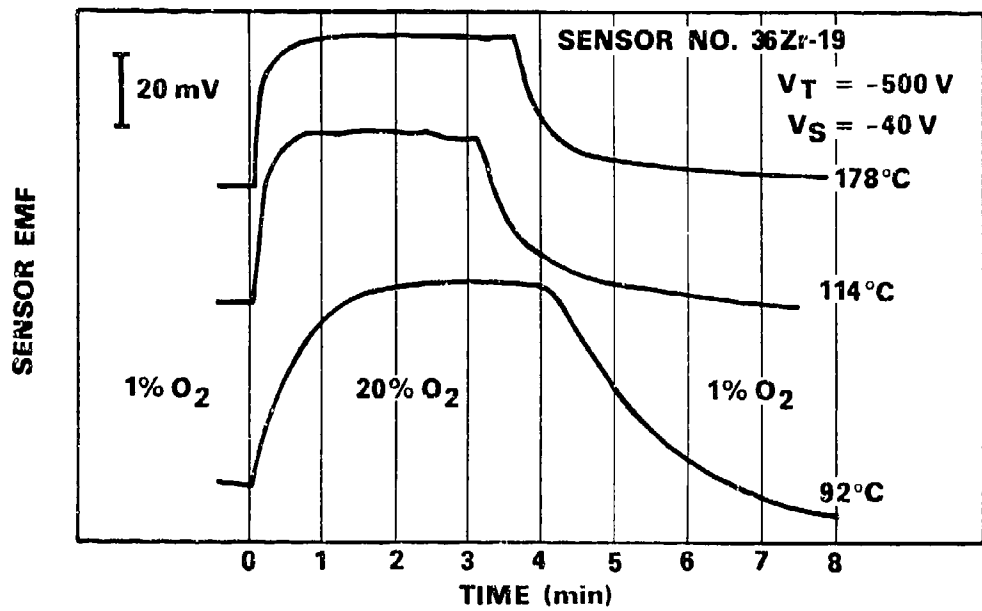
Figure 9 – Response Time Tests

RESPONSE TIME
TEMPERATURE DEPENDENCE
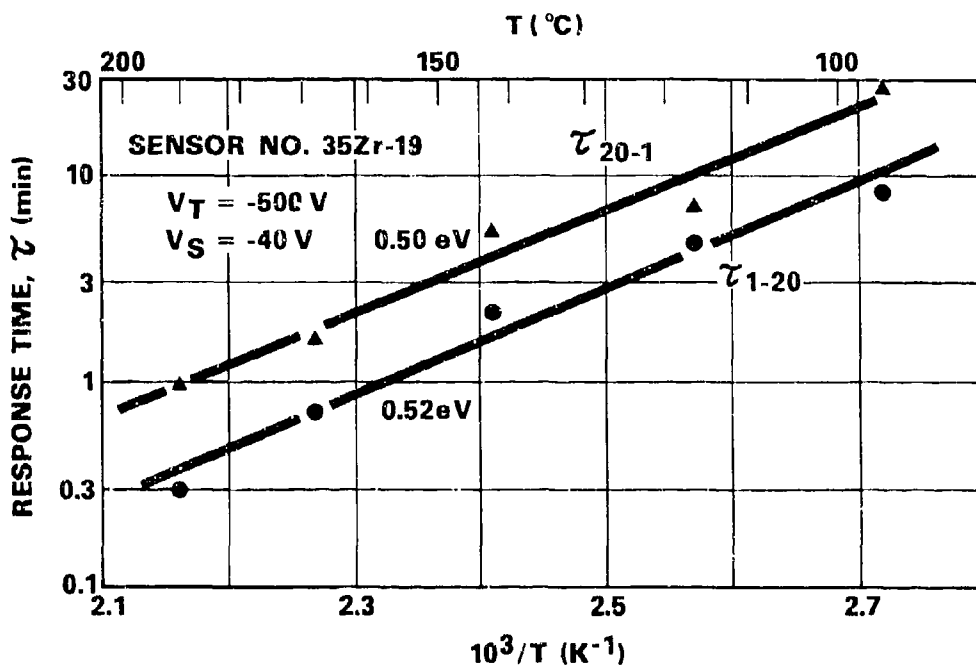
Figure 10 – Response Time
Temperature Dependence –
Sensor No. 35Zr-19

RESPONSE TIME
TEMPERATURE DEPENDENCE
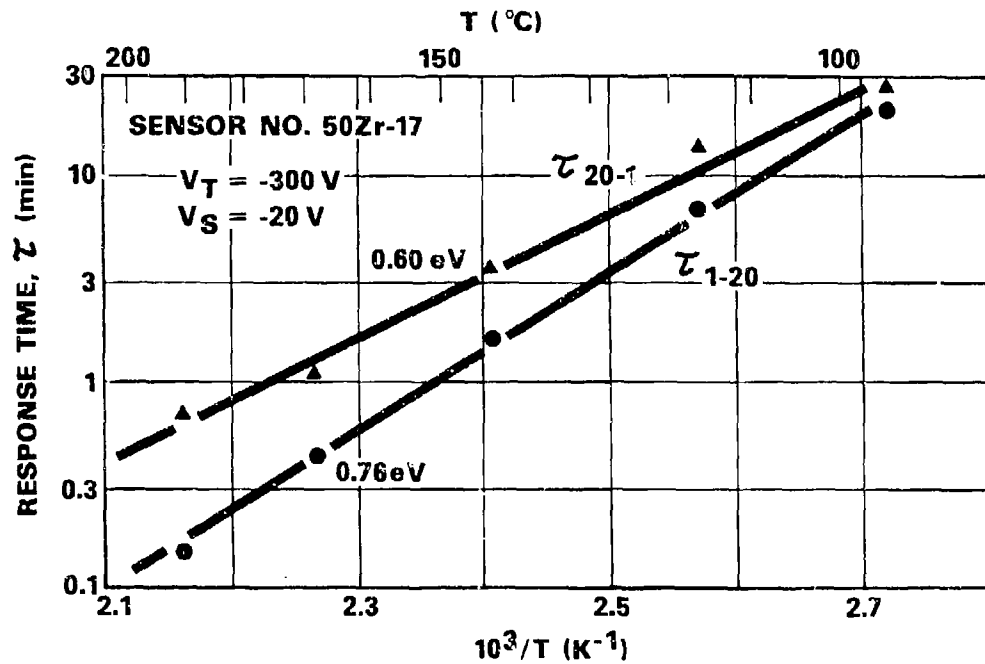
Figure 11 - Response Time
Temperature Dependence –
Sensor No. 50Zr-17

31

TABLE 11

TABULATION OF SENSOR PERFORMANCE DATA

Type	Sputter Run	Film No.[a]	Temp. (°C)	EMF in 1% O_2 (mV)	Typical ΔE_{1-20}[b] (mV)	Electrodes
2	50	17	174	280	29	Pt, sput. 50 nm
		19	186	688	73	Pt, sput. 70 nm
			157	638	70	
			185	–	37	
		20	168	83	27	Pt, sput. 70 nm
			184	–	23	
			220	115	27	
3	35	19	174	1230	40	Pt, sput. 50 nm
		22	157	1448	16	Pt, sput. 70 nm
			179	1063	32	
		24	168	1016	76	Au, sput. 70 nm
			184	–	83	
			228	1034	96	
			183	–	58	
	36	19	174	1360	25	Pt, sput. 50 nm
		22	157	1500	17	Pt, sput. 70 nm
4	41	1-A	150	–	60	Pt paste
			99	–	30	
			186	415	27	
		12	186	666	82	Ag, vapor dep.
		13	177	931	20	Pt, sput. 70 nm
		14	180	1462	35	Pt, sput. 50 nm
			115	1382	34	
		25	182	431	48	Pt paste
			244	424	27	
			179	361	28	
			180	404	31	

TABLE 11 (CONT'D)

Type	Sputter Run	Film No.[a]	Temp. (°C)	EMF in 1% O_2 (mV)	Typical ΔE_{1-20}[b] (mV)	Electrodes
5	42	2-G	186	401	18	Pt paste
		4-G	186	388	18	Pt paste
		13	181	450	68	Pt paste
			244	721	158	
			179	762	76	
		24	188	550	90	Au, vap. dep.
		25	183	442	85	Pt paste
			244	475	68	
			179	402	35	
			180	380	28	
			179	127	22	
7	102	16	122	708	100	Pt, sput. 30 nm
		17	126	1040	69	Pt, sput. 30 nm
		20	122	517	144	Pt, sput. 30 nm
8	103	9	126	1079	48	Pt, sput. 30 nm
	105	2[c]	176	982	27	Pt, sput. 50 nm
			146	970	24	
		3[c]	176	960	26	Pt, sput. 50 nm
			146	976	33	
		7[c]	173	1379	19	Pt, sput. 50 nm
		9[c]	173	1393	32	Pt, sput. 50 nm

[a]Stainless steel substrates except A = alumina and G = glass.

[b]Change in sensor EMF between 1% and 20% O_2 mixtures.

[c]Electrolyte film heat treated before sensor assembly.

changes in EMF larger than those predicted by the Nernst equation. During the course of this program, these problems have been dealt with by:

- changing the gas handling system to reduce unwanted contamination of the test gases.

33

- using minimal amounts of RTV for sensor mounting and recog-
  nizing that it would affect the results until it had outgassed.

- heat treating the electrolyte films before sensor assembly.
  This increases the oxygen content of the electrolyte as dis-
  cussed earlier in this Section.

The effect of increasing temperature on a newly assembled sensor
containing an untreated, oxygen deficient electrolyte is shown in Figure
12. At the lower temperatures, the response is many times Nernstian and
it decreases in magnitude as the temperature is increased.

Heat treating experiments on doped zirconia films indicate that

- the films become more transparent as the oxygen content increases.

- in the neighborhood of 180°C the oxygen imbibition takes place
  over a period of hours and that it has a very strong temperature
  dependence.

The film in sensor 35Zr-24 was much more transparent after the tests
shown in Figure 12 than before it was tested. This suggests that the
decrease in response to nearly the predicted behavior observed at higher
temperatures (at which oxygen imbibition would take place more rapidly
than at 180°C) is due to a decrease in oxygen deficiency of the sensor
electrolyte.

Figures 13-15 present further evidence for this phenomenon. In
Figure 13 the response of a sensor to three 1 hr. gas cycles is shown.
Cycle 1 began shortly after reaching thermal equilibrium at 185°C. The
third and tenth cycles at 185°C show a decreasing response as the thermal
exposure is increased. The vertical positions of the traces for each
cycle are not significant in this figure.

Figure 14 shows the data of Figure 13 plotted in a convenient
form to show how the performance of the sensor approached the per-
formance predicted by the Nernst equation. In Figure 14, ΔE is the
difference between the sensor EMF for any value of P_{O_2} and the EMF
at $P_{O_2} = 0.01$ atm. Figure 15 shows a plot similar to Figure 14 but
for a different sensor at a slightly lower temperature. The results
are qualitatively the same but sensor 42Zr-25 takes much longer to
approach the predicted performance.

d. Current State of Sensor Performance in O_2/N_2 Atmospheres

The best performance results obtained during Phase 1 are shown in
Figures 16-18. Sensor response is very close to the predicted (Nernstian)
response and much more reproducible. The electrolyte film of this sensor
was heat treated in air at 450°C for 15 minutes before sensor assembly.
The data shown in Figures 16-18 demonstrate the following points:

34

EFFECT OF INCREASING TEMPERATURE ON NEW SENSOR
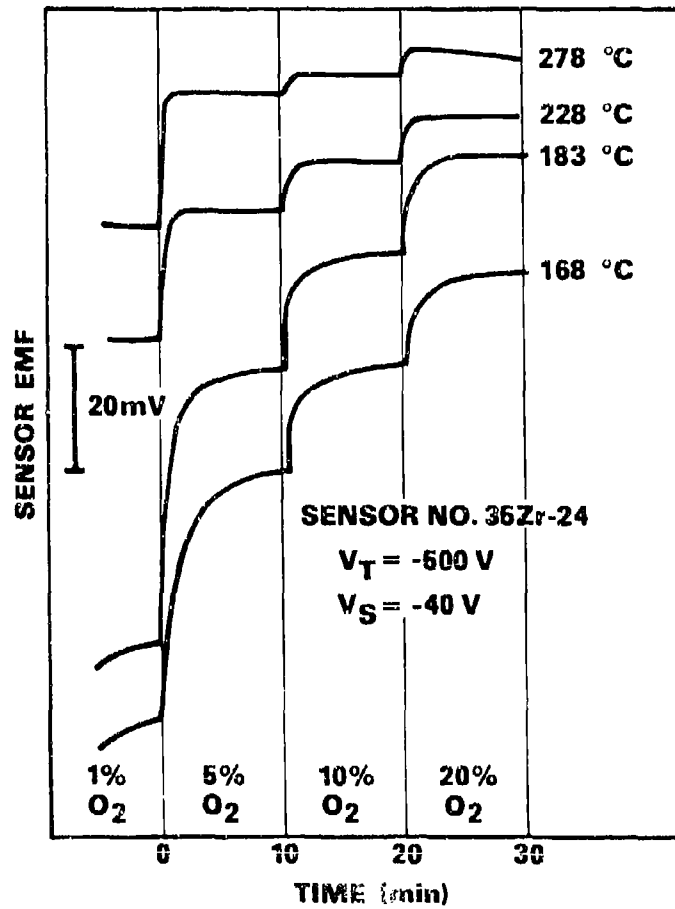
Figure 12 – Effect of Increasing Temperature on New Sensor

35

SENSOR RESPONSE AT INCREASING THERMAL EXPOSURES
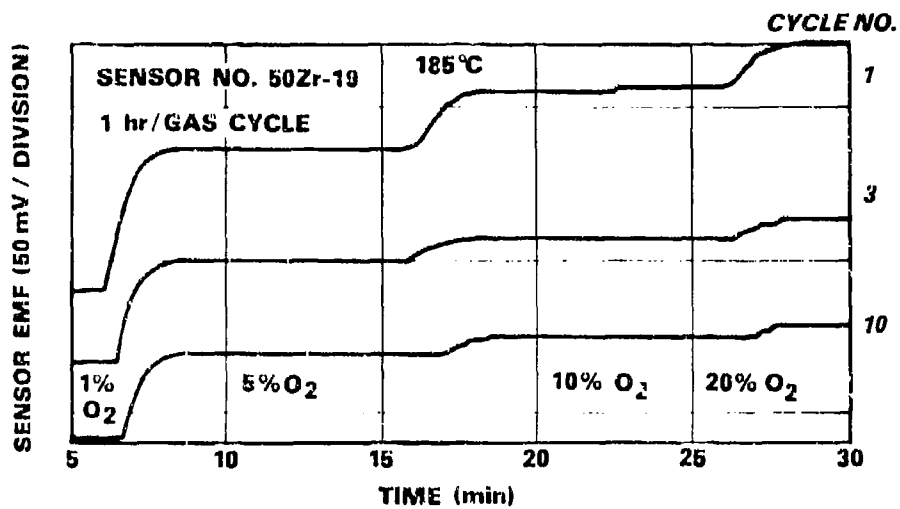
Figure 13 - Sensor Response at
Increasing Thermal Exposures -
Sensor No. 50Zr-19

36

SENSOR RESPONSE AT INCREASING THERMAL EXPOSURES

Figure 14 – Analysis of Sensor
Response at Increasing Thermal
Exposures – Sensor No. 50Zr-19

SENSOR RESPONSE AT INCREASING THERMAL EXPOSURES

SENSOR NO. 42Zr-25   179 °C

$V_T = -500$ V

$V_S = -80$ V

ΔE (mV)

1 hr. / GAS CYCLE

CYCLE NO.

PREDICTED PERFORMANCE

OXYGEN PARTIAL PRESSURE (atm)
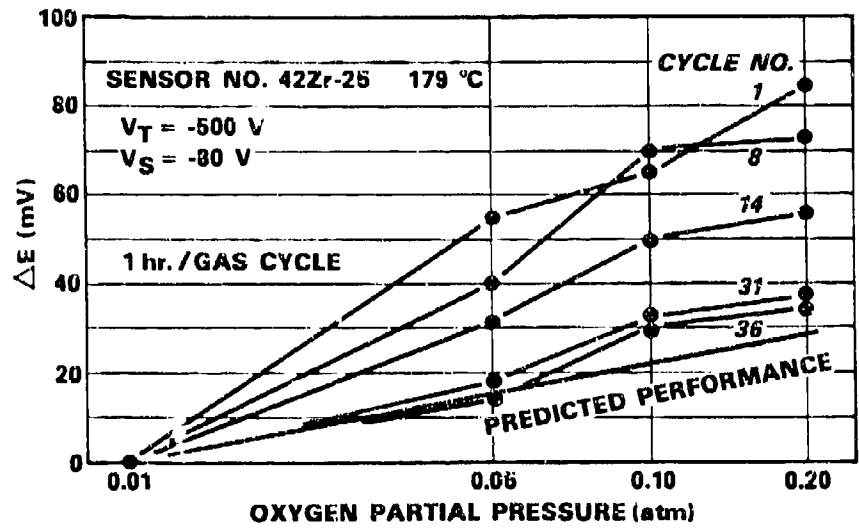
Figure 15 - Analysis of Sensor
Response at Increasing Thermal
Exposures - Sensor No. 42Zr-25

RESPONSE OF SENSOR WITH HEAT TREATED ELECTROLYTE
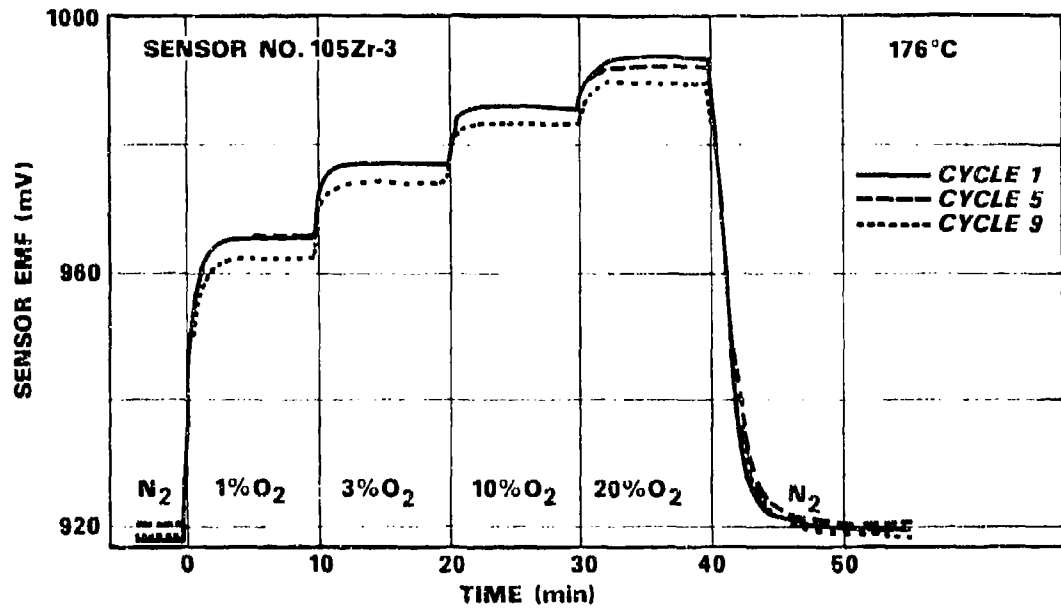
Figure 16 - Response of Sensor with
Heat Treated Electrolyte -
Absolute Reproducibility

39

RESPONSE OF SENSOR WITH HEAT TREATED ELECTROLYTE
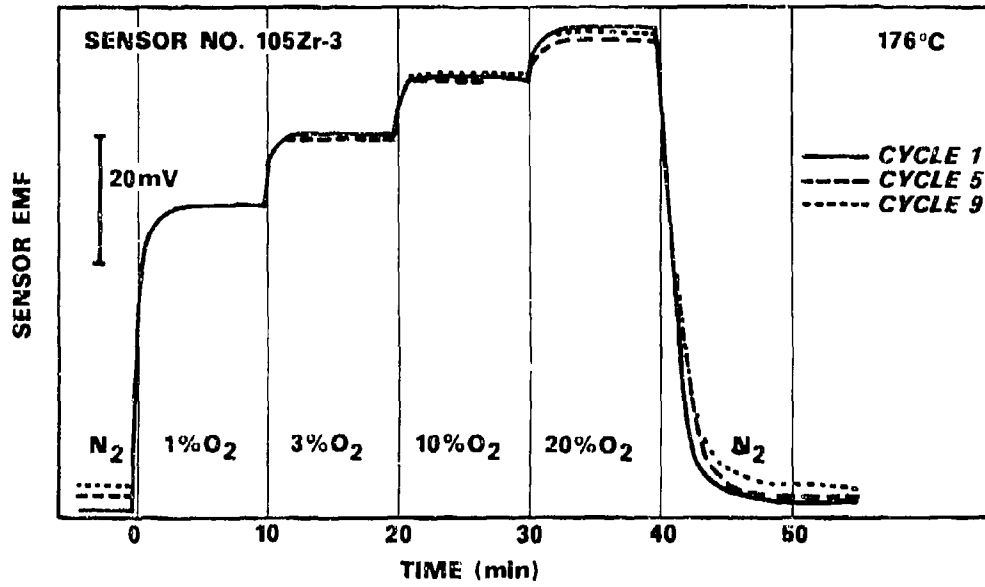
Figure 17 - Response of Sensor with
Heat Treated Electrolyte -
Reproducibility of EMF Changes

RESPONSE OF SENSOR WITH HEAT TREATED ELECTROLYTE
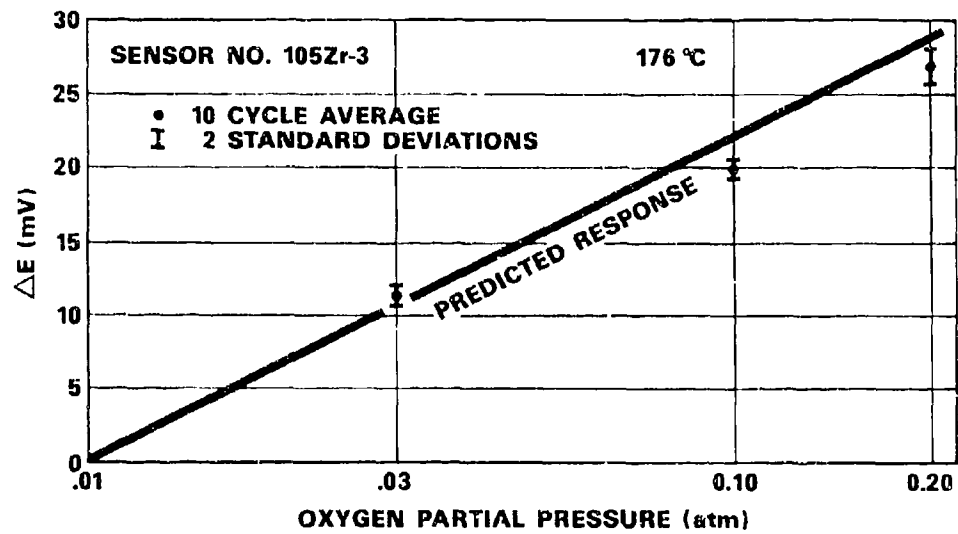
Figure 18 – Analysis of the
Response of Sensor with Heat
Treated Electrolyte

41

(i)   The absolute voltage reproducibility of this sensor during 10 one hour cycles is shown in Figure 16. The total voltage drift in performance at 0.03 atm O_2 is less than 4 mV or ~0.01 atm O_2.

(ii)   The normalized reproducibility or the reproducibility in ΔE is shown in Figure 17 where the data are normalized to the response at 1% O_2 concentration. The reproducibility at 0.03 atm O_2 is within ~1 mV or ~0.003 atm O_2.

(iii)   The comparison between the actual and predicted performance of this sensor is shown in Figure 18. The data from ten consecutive gas cycles were analyzed to obtain the average values and standard deviations of ΔE for each gas mixture.

The sensor performance shown in Figures 16-18 represents the dramatic improvement in oxygen sensor performance made during Phase 1 of this program.

5.   CONTAMINANT EFFECTS ON SENSOR PERFORMANCE

Under the contract requirements, the effects on sensor performance were determined for gaseous H_2O, CO_2, NO_2, SO_2, and C_3H_8 contaminants at specified concentration levels. The effects of contaminants on sensor performance were studied primarily at temperatures near 180°C, although some lower temperature tests were made. In general, the sensor EMF was altered to some degree by the presence of each contaminant. In some cases the change in sensor output was substantial, but in no case was the sensor damaged by this exposure. Generally, the effect of gaseous contaminants on sensor performance decreased with decreasing temperature.

The normal method for determining the effects of gaseous contaminants on sensor performance was to alternately expose the sensor to an O_2/N_2 mixture and a mixture containing the same O_2 concentration plus the contaminant gas. This was done at times within a normal O_2/N_2 cycle.

a.   Water Vapor Contaminant Tests

The contaminant gas mixture used for these tests contained 3.04% O_2 and 265 ppm H_2O. A typical result is shown in Figure 19. The effect of H_2O was determined for a total of seven sensors. A summary of the results is given in Table 12. For each sensor, the EMF at P_{O_2} = 0.03 atm using a contaminant free gas is given. The change in EMF, ΔE_{con}, caused by the contaminant and the change in EMF, ΔE_{1-3} due to a change in P_{O_2} from 0.01 to 0.03 atm are also shown. The ratio of $\Delta E_{con}/\Delta E_{1-3}$ is shown in the following column. The final column shows the error induced by

WATER VAPOR CONTAMINANT TEST
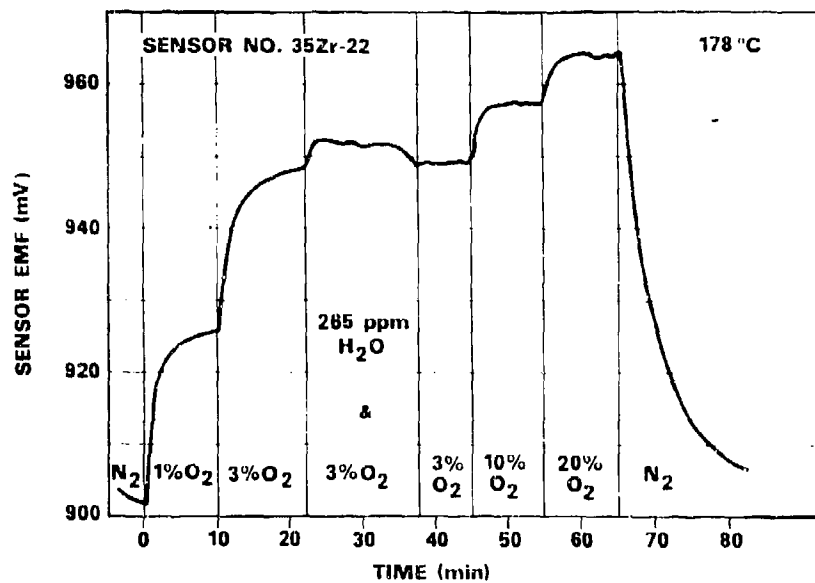
Figure 19 — Water Vapor
Contaminant Test

43

TABLE 12

EFFECT OF 265 ppm WATER VAPOR ON THE EMF OF
SEVERAL SENSORS AT P_{O_2} = 0.03 atm AND T ~180°C

Type	Sensor	EMF (mV)	ΔE_{con} (mV)	ΔE_{1-3} (mV)	$\dfrac{\Delta E_{con}}{\Delta E_{1-3}}$	Error (atm O_2)
2	50Zr-17	455	+0.3	23	0.013	+0.0004
3	35Zr-19	1320	+0.5	22	0.023	+0.0008
	35Zr-22	950	+3.0	22	0.14	+0.0048
	35Zr-24	870	−2.0	40	−0.050	−0.0017
	36Zr-19	1350	+0.5	40	0.013	+0.0004
4	41Zr-13	820	+2.0	12	0.17	+0.0060
5	42Zr-25	140	+0.5	10	0.05	+0.0017

the contaminant in % O_2 concentration for the sensor used as an oxygen
sensor. For example, for sensor 50Zr-17 the H_2O vapor caused a change
of +0.3 mV, which produced an oxygen concentration reading by the sensor
which was 0.0004 atm higher than the actual oxygen concentration. The error
values were calculated with the Nernst equation by first finding ηt_i
from the ΔE_{1-3} value.

$$\Delta E_{1-3} = \eta t_i \frac{RT}{4F} \ln \frac{P_{O_2} \ (= .03 \text{ atm})}{P_{O_2} \ (= .01 \text{ atm})}$$

or

$$\eta t_i = \frac{4F}{RT} \frac{\Delta E_{1-3}}{\ln 3}$$

(The factor η takes into account the larger than Nernstian voltage
changes measured using non-stoichiometric films.)

Then the apparent oxygen partial pressure $P_{O_2}^a$ was calculated using the
Nernst equation again

$$P_{O_2}^a = P_{O_2} \exp \left(\frac{4F \ \Delta E_{con}}{RT \eta t_i} \right)$$

or

$$P_{O_2}^a = P_{O_2} \exp \left(\frac{\Delta E_{con}}{\Delta E_{1-3}} \ln 3 \right)$$

The error can now be calculated.

$$\text{Error (atm } O_2) = P_{O_2}^a - 0.03 \text{ atm}$$

The results show that for all sensors but one, ΔE_{con} is positive and the maximum error induced by 265 ppm H_2O was 0.006 atm in the oxygen concentration. .

b. CO_2 Contaminant Tests

The contaminant gas mixture used for these tests contained 2.69% O_2 and 10.02% CO_2. A typical result is shown in Figure 20. The effect of CO_2 was determined for a total of seven sensors and a summary of the results is given in Table 13. The type of information is the same as that presented in Table 12 for H_2O tests.

The results show that ΔE_{con} is negative for all but two sensors and that the maximum error induced by 10% CO_2 was -0.014 atm in the oxygen concentration.

TABLE 13

EFFECT OF 10% CO_2 ON THE EMF OF SEVERAL
SENSORS AT P_{O_2} = 0.03 atm AND T $\sim$ 180°C

Type	Sensor	EMF (mV)	ΔE_{con} (mV)	ΔE_{1-3} (mV)	$\dfrac{\Delta E_{con}}{\Delta E_{1-3}}$	Error (atm O_2)
2	50Zr-17	430	-12	24	-0.50	-0.013
3	35Zr-19	1310	-12	23	-0.52	-0.013
	35Zr-22	950	-3	22	-0.14	-0.004
	36Zr-19	1320	-19	33	-0.56	-0.014
4	41Zr-13	835	-6	14	-0.43	-0.011
	41Zr-25	280	+1	8	+0.12	+0.004
5	42Zr-25	150	+1	8	+0.12	+0.004

c. NO_2 Contaminant Tests

The contaminant mixture used for these tests contained 2.90% O_2 and 0.098% NO_2. A typical result is shown in Figure 21. The effect of NO_2 was determined for a total of five sensors and a summary of the results is given in Table 14. The error induced by NO_2 is large and was not calculated. Sensors will recover from the effects of NO_2 over a sufficient period of time. The large slope on the 10% O_2 and 20% O_2 segments of Figure 21 is due to this recovery. Notice that the EMF is lower than the EMF at P_{O_2} = 0.03 atm before NO_2 exposure. Nonetheless the sensor does continue to respond to changes in P_{O_2} even immediately after NO_2 exposure.

CARBON DIOXIDE CONTAMINANT TEST
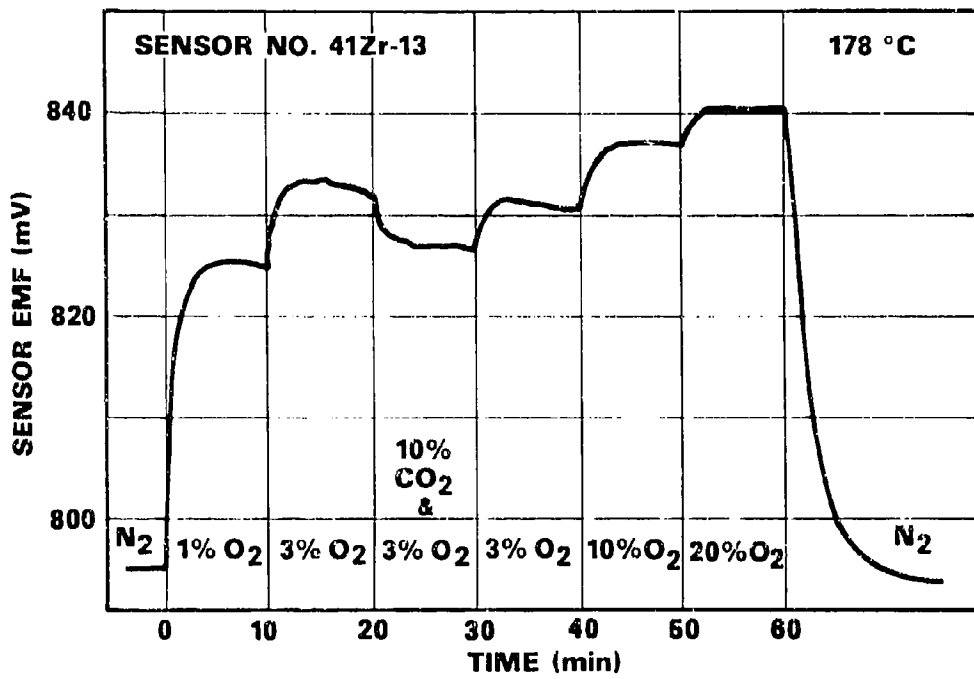
Figure 20 – Carbon Dioxide
Contaminant Test

NITROGEN DIOXIDE CONTAMINANT TEST
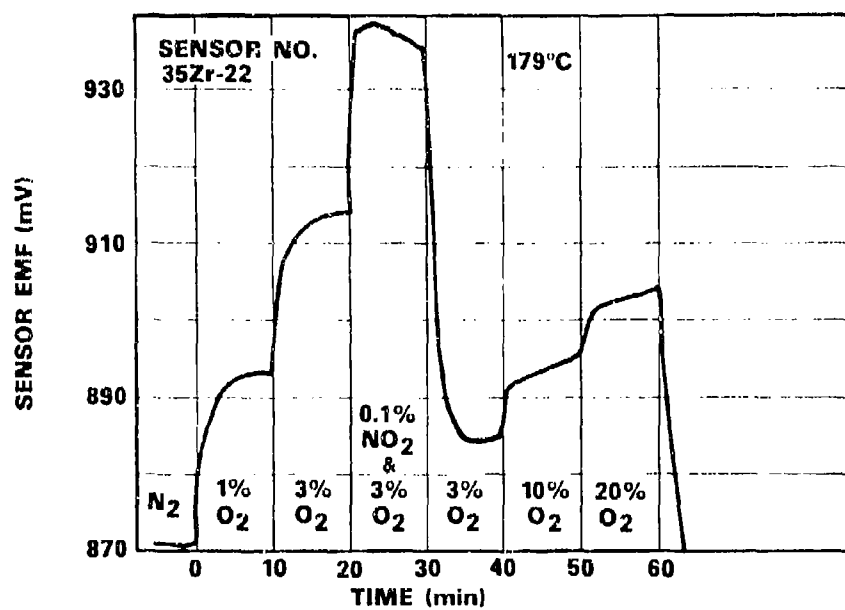
Figure 21 — Nitrogen Dioxide Contaminant Test

TABLE 14

EFFECT OF 0.1% NO$_2$ ON THE EMF OF SEVERAL
SENSORS AT P$_{O_2}$ = 0.03 atm AND T $\sim$ 180°C

Type	Sensor	EMF (mV)	ΔE_{con} (mV)	ΔE_{1-3} (mV)	$\frac{\Delta E_{con}}{\Delta E_{1-3}}$
2	50Zr-17	430	+120	9	+13.3
3	35Zr-19	1340	+72	15	+4.8
	35Zr-22	900	+47	21	+2.24
	36Zr-19	1390	+120	15	+8.0
4	41Zr-13	800	+120	10	+12.0

d. SO$_2$ Contaminant Tests

The contaminant gas mixture used for these tests contained 3.24% O$_2$ and 0.01% SO$_2$. A typical result is shown in Figure 22. The effect of SO$_2$ was determined for a total of five sensors and a summary of the results is given in Table 15.

The initial increase in EMF upon exposure to SO$_2$, followed by a change to an equilibrium decrease in EMF is characteristic of sensor response to SO$_2$. The values given in Table 15 are equilibrium values and are in all cases negative. Errors in O$_2$ concentration range from -.027 atm out of 0.03 atm total to just -0.004 atm. There is no lingering effect from SO$_2$ as there is for NO$_2$.

TABLE 15

EFFECT OF 0.01% SO$_2$ ON THE EMF OF SEVERAL
SENSORS AT P$_{O_2}$ = 0.03 atm AND T $\sim$ 180°C

Type	Sensor	EMF (mV)	ΔE_{con} (mV)	ΔE_{1-3} (mV)	$\frac{\Delta E_{con}}{\Delta E_{1-3}}$	Error (atm O$_2$)
2	50Zr-17	448	-39	18	-2.2	-0.027
3	35Zr-19	1370	-50	26	-1.9	-0.026
	35Zr-22	910	-25	18	-1.4	-0.023
	36-Zr-19	1340	-4	28	-0.14	-0.0044
4	41Zr-13	705	-4	9	-0.44	-0.012

SULFUR DIOXIDE CONTAMINANT TEST
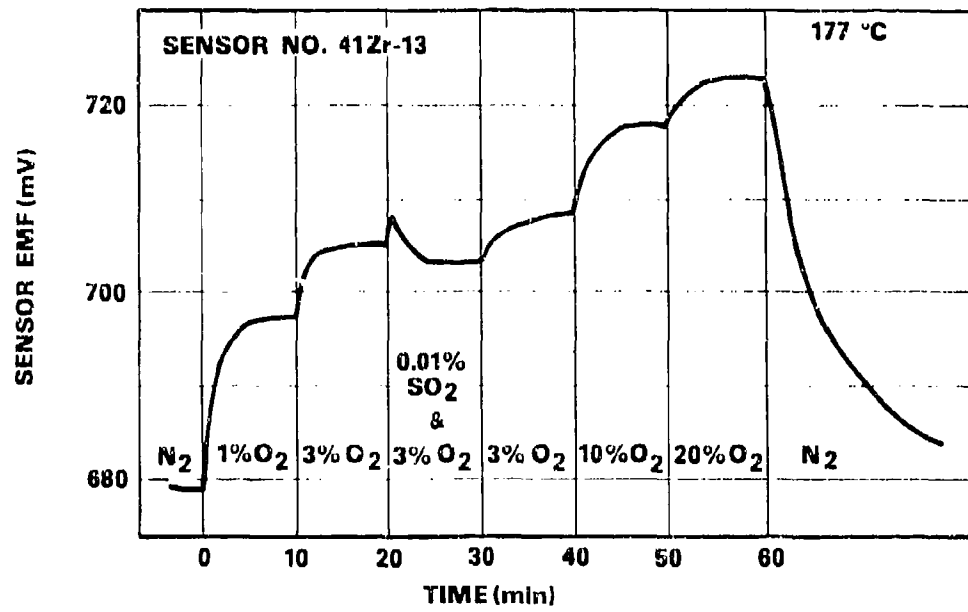
Figure 22 - Sulfur Dioxide
Contaminant Test

e. C_3H_8 Contaminant Tests

The contaminant gas mixture used for these tests contained 1.08% O_2 and 1.52% C_3H_8. A typical result is shown in Figure 23. The effect of C_3H_8 was determined for a large number of sensors and a summary of the results for seven of them is given in Table 16. In Figure 23, the larger EMF after exposure to propane than before is a dynamic response. That is, if P_{O_2} had been maintained at 3% for a sufficient period of time the EMF would have returned to its pre-exposure value. This statement is based on several incidences in which such observations were made. This overshoot and subsequent return to equilibrium was not understood until further experiments, to be described below, were carried out. Those experiments showed that the EMF increases for very small propane concentrations. This suggests that the overshoot is due to a small residual amount of propane in the test chamber which is slowly flushed away causing the EMF to return to equilibrium.

TABLE 16

EFFECT OF 1.5% C_3H_8 ON THE EMF OF SEVERAL
SENSORS AT P_{O_2} = 0.01 atm AND T ∿180°C

Type	Sensor	EMF (mV)	ΔE_{con} (mV)	ΔE_{1-3} (mV)	$\frac{\Delta E_{con}}{\Delta E_{1-3}}$
2	50Zr-17	448	-175	15	-11.7
3	35Zr-19	1320	-275	25	-11.0
	35Zr-22	900	-(>100)	26	-(>3.8)
	36Zr-19	1350	-225	25	-9.0
4	41Zr-13	702	-(>100)	7	-(>14.3)
	41Zr-25	280	-46	10	-4.6
5	42Zr-25	150	-37	10	-3.7

Additional experiments were performed to explain the apparent inconsistency between the current results and the results of a preliminary experiment with propane that was done before this contract period commenced. The additional testing produced several important results.

(1) The response time to changes in P_{O_2} is generally faster in the presence of propane and in some cases is very much faster. No systematic data were taken but the data in Table 17 are indicative of the response times that can be obtained in the presence of propane. These can not be compared directly with the data of Figures 10 and 11 because of the

50

PROPANE CONTAMINANT TEST
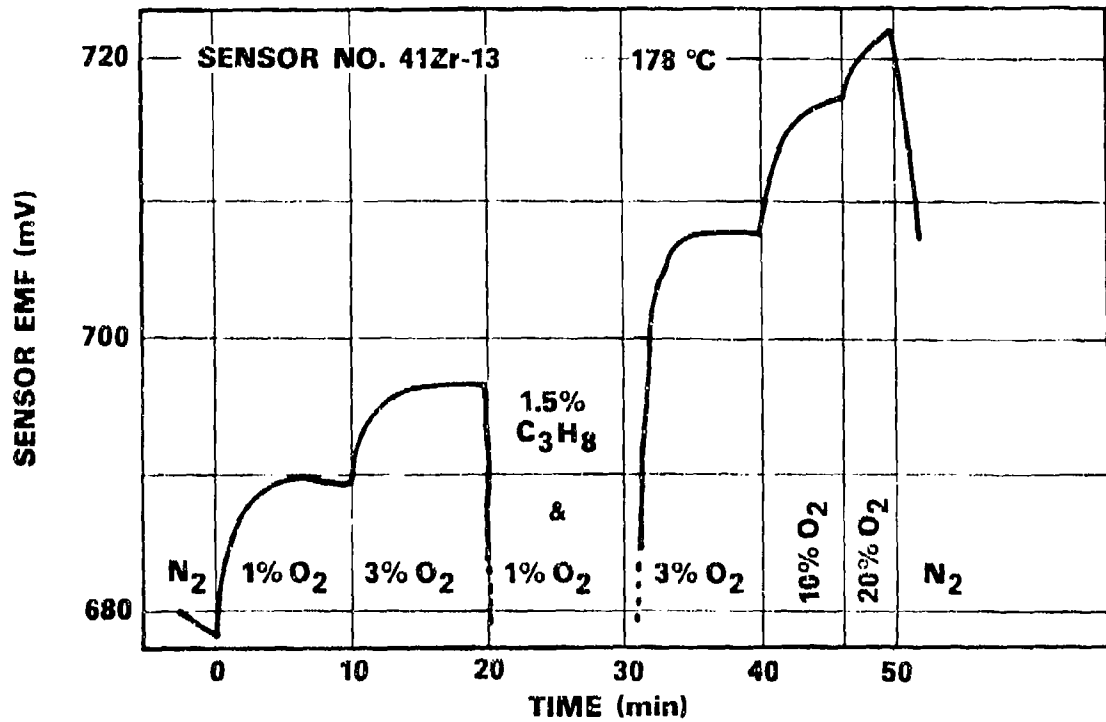
Figure 23 - Propane
Contaminant Test

51

differences in the magnitude of the change in P_{O_2}. However, the response times in Table 17 are smaller than the response times for any change in P_{O_2} made during normal testing in O_2/N_2 atmospheres.

TABLE 17

SENSOR RESPONSE TIMES IN THE PRESENCE
OF PROPANE AT 173°C

Sensor	P_{O_2} changes between 0.002 and 0.163 atm $P_{C_3H_8} = .0108$ atm		P_{O_2} changes between 0.007 and 0.065 atm $P_{C_3H_8} = 0.003$ atm	
	τ_{inc}^{a} (min)	τ_{dec}^{b} (min)	τ_{inc}^{a} (min)	τ_{dec}^{b} (min)
36Zr-19	0.060	0.23	0.096	0.16
50Zr-17	0.13	0.42	0.17	0.27

[a] Response time for increase in P_{O_2} between stated values.
[b] Response time for decrease in P_{O_2} between stated values.

(ii) The magnitude of the change in EMF due to a change in P_{O_2} is larger in the presence of propane than in uncontaminated O_2/N_2 mixtures. Examples of this effect are shown in Figures 24 and 25. Figure 24 shows the response of a sensor to changes in P_{O_2} at two different propane concentrations. These data are plotted in Figure 25 against ln P_{O_2} and compared with the change in EMF predicted by the Nernst equation. The response of this sensor in uncontaminated O_2/N_2 atmospheres is very close to Nernstian, that is, this effect is clearly due to the presence of propane and not to the oxygen deficiency of the electrolyte discussed in Section IV-4.

(iii) For propane concentrations up to 35% and $P_{O_2}/P_{C_3H_8}$ ratios less than 1 at 140°C or less than 10 at 180°C, the sensor EMF values fall in a narrow, montonically changing band when plotted against $P_{O_2}/P_{C_3H_8}$. An example of the type of data obtained is shown in Figure 26. These data were obtained by mixing the 1% O_2, 1.5% C_3H_8 mixture with the 1% O_2 mixture at various ratios. Other data have been obtained by mixing the 1%, 3%, and 10% O_2 mixtures with pure C_3H_8 in several different ratios. Those data, when plotted similarly to those in Figure 26 fall

Figure 24 - Oxygen Sensing in the
Presence of Propane

OXYGEN SENSING IN THE PRESENCE OF PROPANE

SENSOR NO. 35Zr-19

$P_{C_3H_8} = 0.0076$ atm

174 °C

SENSOR EMF (mV)

P_{O_2} (atm)   0.005   0.01   0.02   0.055   0.105   0.005

$P_{O_2}/P_{C_3H_8}$ 0.67   1.32   2.63   7.24   13.82   0.67

TIME (min)

SENSOR NO. 35Zr-19

$P_{C_3H_8} = 0.0107$ atm

174 °C

SENSOR EMF (mV)

P_{O_2} (atm)   0.007   0.01   0.016   0.037   0.066   0.007

$P_{O_2}/P_{C_3H_8}$ 0.65   0.93   1.49   3.42   6.17   0.65

TIME (min)

53
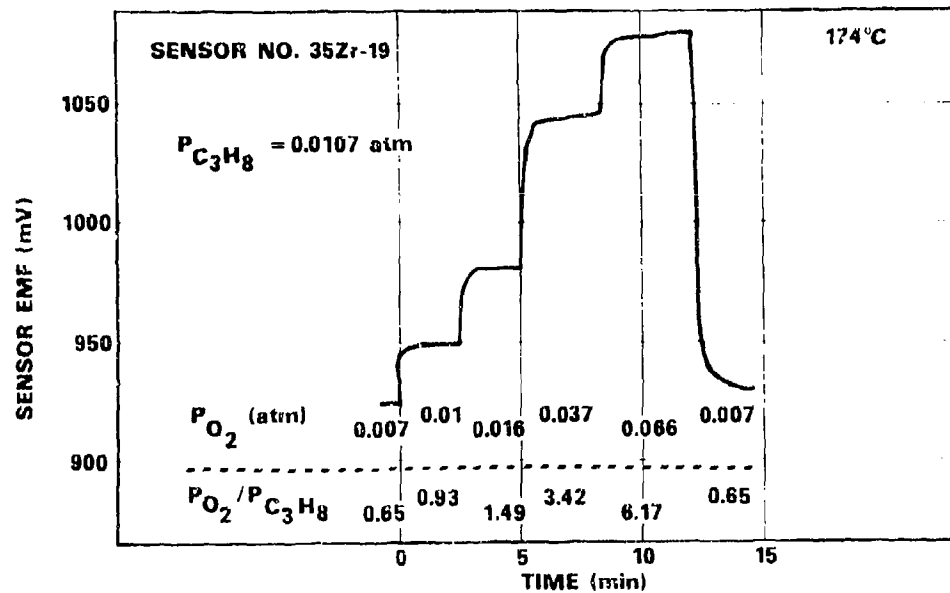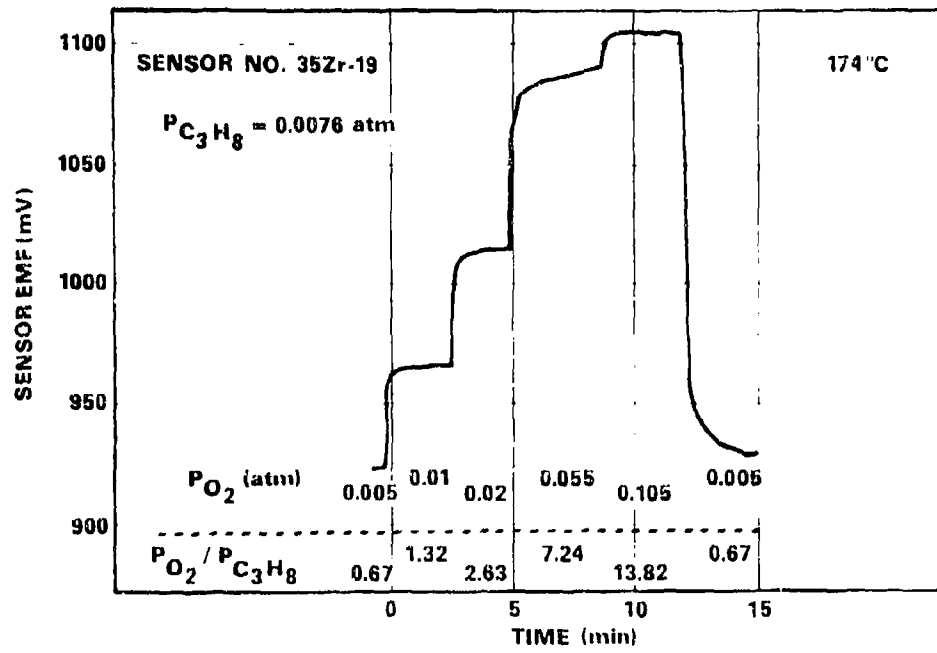
OXYGEN SENSING
IN THE PRESENCE OF PROPANE
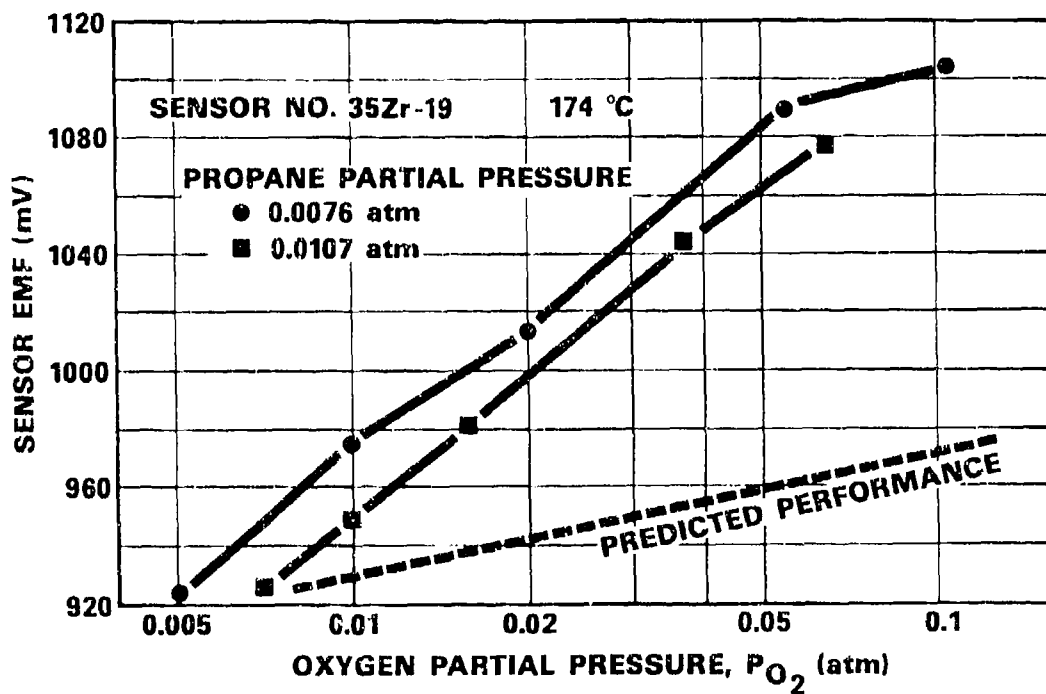
Figure 25 - Analysis of Oxygen
Sensing in the Presence
of Propane

DEPENDENCE OF SENSOR EMF ON OXYGEN-TO-PROPANE RATIO
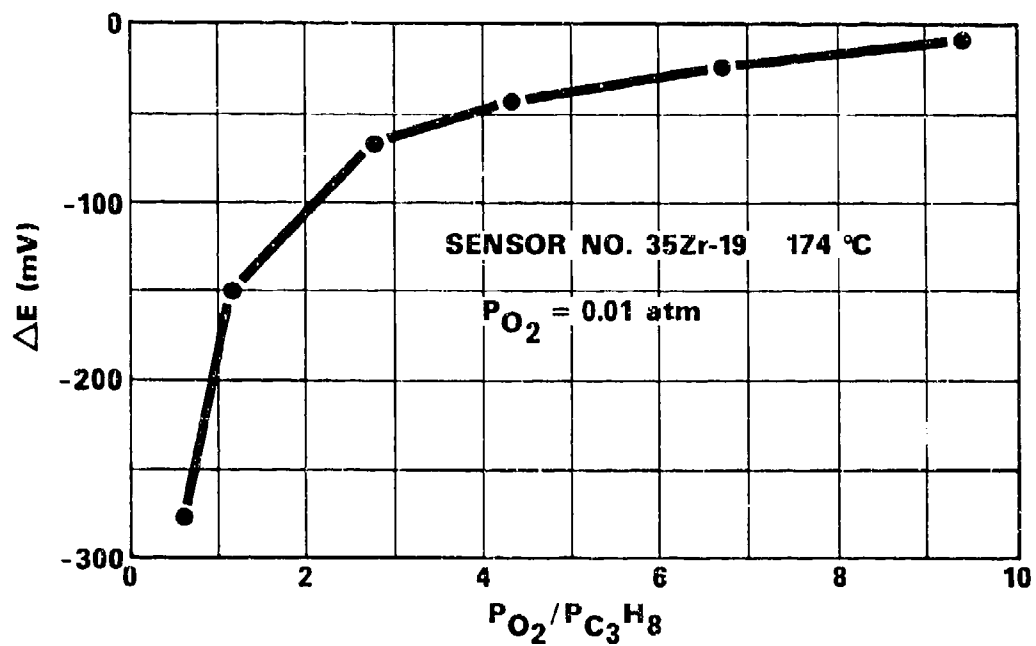
Figure 26 – Dependence of Sensor
EMF on Oyxgen-to-Propane Ratio

in a narrow band with a similar shape. The data are not monotonic for very large values of $P_{O_2}/P_{C_3H_8}$ (small propane concentrations) as discussed earlier. However, the downturn at large $P_{O_2}/P_{C_3H_8}$ is typically only a few millivolts compared to the hundreds of millivolts change as $P_{O_2}/P_{C_3H_8}$ approaches zero.

SECTION V

OXYGEN SENSOR PERFORMANCE - PHASE II

1. INTRODUCTION

The technical effort on the second phase of this program was begun following completion of the Phase I requirements. This effort was directed toward testing the sensors developed in Phase 1 under ullage conditions simulated in a laboratory test station. In a series of tests, the effects of fuel (JP-4), tank sealant, water vapor, and reduced temperatures and pressures on sensor performance were determined. These tests were designed to determine if a sensor can operate in a fuel tank ullage space and to determine what design constraints will be required for an operational sensor.

In addition to the Phase 11 test results, the oxygen sensing performance of five sensors supplied to AFAPL/SFH is presented in this section.

2. EFFECT OF FUELS

a. Liquid Fuel (JP-4) Dropped Onto an Operating Sensor

This test was conducted with JP-4 fuel provided by AFAPL/SFH to simulate either the effect of fuel sloshing onto an operating sensor or the effect of fuel mist droplets in the ullage space depositing on the sensor.

(i) Experimental Procedure. The sensor was placed in a glass vessel inside an oven. Tubes attached to the sidewall of the vessel were used to permit a gas flow and as feedthroughs for sensor and thermocouple leads. The leads were sealed into the tubes with RTV. The thermocouple used to determine sensor temperature was clamped to the outer part of the sensor assembly (see Figure 5b). During these tests, a constant flow of a 10% O_2, 90% N_2 gas mixture was maintained in the glass vessel.

The fuel (JP-4) was dropped onto the sensor with a pipette which extended through a sealed hole in the top of the glass vessel. The pipette could be removed for refilling whenever necessary. Visual observation confirmed that the fuel dropped directly onto the sensor.

(ii) Results. The results of two fuel drop tests are shown in Table 18. In both cases sensor EMF drops by more than 50 mV and recovers to the original EMF in roughly three minutes. The temperature of the sensor also dropped during the test as a result of exposure to the colder fuel drop and fuel evaporation from the sensor surface. The temperatures indicated in Table 18 are those of the outer part of the sensor package and probably indicate a smaller temperature change than

TABLE 18

DROPPING LIQUID FUEL ONTO AN OPERATING SENSOR

Sensor No. 105Zr-10 was used for this test. A constant flow of a 10% O_2, 90% N_2 mixture was maintained.

	Test No. 1						
EMF (mV)	680	618	652	666	673	679	683
T^a (°C)	161	156				159	
Time^b(s)	*	0	40	80	120	160	200

	Test No. 2						
EMF (mV)	705	650	691	697	701	703	706
T^a (°C)	175		173			174	
Time^b(s)	*	0	40	80	120	160	200

[a] Temperature of outer part of sensor assembly. The actual temperature of the active elements of the sensor was probably lower than the measured temperature during fuel evaporation and for a period of time after evaporation was completed.

[b] Time equals zero when fuel hits sensor.

*EMF and temperature before dropping fuel onto sensor.

actually occurs at the gas sensing electrode. Consequently, the measured recovery time of three minutes probably reflects the time required for thermal re-equilibration in this test configuration of the sensor. It is expected that control of the sensor temperature by attachment of a heating element directly to the sensor would reduce the recovery time.

The results of this test indicate that occasional sloshing of fuel onto a sensor should have no long term deleterious effect on sensor performance.

b. Effect of Soaking Sensors in Fuel (JP-4)

Three sensors were soaked in JP-4 at room temperature for a period of 24, 48, or 96 hours to determine the effect of long-term contact with liquid fuel.

(i) Experimental Procedure. Three sensors were tested in O_2/N_2 enviroments using the test chamber shown in Figure 6b. They were then removed from the test chamber and positioned so that the outer shell of the sensor assembly would contain the liquid fuel. Enough fuel was placed in the sensor assembly so that the oxide film, the electrodes, and the electrode attachment medium were immersed. The sensor was placed in a closed container to prevent evaporation of the fuel. After the prescribed time period, the fuel was poured out of the sensor and the oxide film-electrode surface was flushed with clean fuel. The sensor was then retested in O_2/N_2 enviroments.

(ii) Results of 24 Hour Soak. The results of measurements on sensor No. 105Zr-3 before and after soaking in JP-4 fuel for 24 hours are shown in Table 19. In each case the sensor was tested with 1% O_2, 3% O_2, 10% O_2, and 20% O_2 with 10 minutes per gas mixture. Both the sensor EMF and the change in EMF with changing P_{O_2} (ΔE) were varied by at most 4 mV by the fuel soak. Following the soaking period the sensor had a response time of about 6 minutes. With the slower response time after soaking, the sensor EMF did not fully equilibrate at the 1% O_2 level. The extrapolated EMF value is clearly lower than the 1018 mV listed in Table 19.

Based on these results, it is clear that a 24 hour submersion in JP-4 fuel did not destroy the sensing ability nor substantially affect the magnitude of the EMF of this sensor. The only deleterious effect of the fuel soak was an increase in the response time of the sensor.

(iii) Results of 48 Hour Soak. Sensor No. 105Zr-6 was soaked for 48 hrs in JP-4 and the results before and after soaking are shown in Table 20. The change in EMF values is greater here (up to 23 mV) than in the case of the sensor soaked for 24 hrs. The leads had to be re-attached in order to get an acceptable response. As in the case of the 24 hour fuel soak, the sensing ability of the device was not destroyed.

(iv) Results of the 96 Hour Soak. Sensor No. 105Zr-2 was soaked for 96 hrs in JP-4 and the results before and after soaking are shown in Table 21. In this case, the change after soaking was substantial (∼350 mV). The sensing ability was not destroyed but the EMF changed

59

TABLE 19

EFFECT OF 24 HOUR JP-4 SOAK

Sensor No. 105Zr-3

P_{O_2}	Pre-Soak[a]		Post-Soak[b]		Nernstian[c]
	EMF	ΔE[d]	EMF	ΔE[d]	ΔE[d]
(atm)	(mV)	(mV)	(mV)	(mV)	(mV)
0.01	1013	−33[e]	1018	−24[e]	−29
0.03	1021	−25	1020	−22	−18
0.10	1035	−11	1032	−10	−7
0.20	1046	0	1042	0	0

[a] At 168°C.

[b] At 176°C.

[c] At 172°C

[d] Note that the 0.20 atm EMF is used as reference. The 0.01 atm values are not equilbrium values in all cases.

[e] The difference in pre- and post-soak values is primarily due to a decrease in the response time after soaking. The extrapolated equilibrium values are more nearly equal. Compare with the ΔE values at other O_2 pressure.

TABLE 20

EFFECT OF 48 HOUR JP-4 SOAK

Sensor No. 105Zr-6

P_{O_2}	Pre-Soak[a]		Post-Soak[b]		Nernstian[c]
	EMF	ΔE	EMF	ΔE	ΔE
(atm)	(mV)	(mV)	(mV)	(mV)	(mV)
0.01	677	−51	700	−39	−29
0.03	694	−34	711	−28	−18
0.10	709	−19	731	−8	−7
0.20	728	0	739	0	0

[a] At 172°C.

[b] At 177°C. The leads had to be reattached in order to take these data.

[c] At 174°C.

TABLE 21

EFFECT OF 96 HOUR JP-4 SOAK

Sensor No. 105Zr-2

P_{O_2}	Pre-Soak[a]		Post-Soak[b]		Nernstian[c]
	EMF	ΔE	EMF	ΔE	ΔE
(atm)	(mV)	(mV)	(mV)	(mV)	(mV)
0.01	788	−32	1140	−52	−29
0.03	798	−22	1162	−30	−18
0.10	812	−8	1168	−24	−7
0.20	820	0	1192	0	0

[a] At 174°C.

[b] At 172°C. These data are for a different electrode than the pre-soak data.

[c] At 173°C.

62

significantly and the output was noisy after soaking. It was necessary to utilize a different electrode after the fuel exposure than the one which was used initially. The response time was also approximately 6 minutes after this test but equilibrium EMF values were obtained.

(v)   Summary of Fuel Soak Test Results. In the performance of these tests, problems associated with the lead attachment techniques described in Section III-5 arose. Several lead attachments failed during the longer soak tests and different electrodes on the same sensor were used. The use of commercial lead attachment techniques should eliminate these failures. The net results of the fuel tests including the fuel drop experiment indicate that this type of sensor can withstand occasional, short-term exposure to liquid fuels during operation or non-operation. Long-term exposure, however, appears to have an adverse effect on them and some protection against such exposure would have to be provided in an inerting system using this type of sensor.

3.   ALTITUDE SIMULATION TESTS

The effect of altitude on sensor performance was simulated by measuring sensor output in the total pressure range of ~3 to 14.7 psia.

a.   Experimental Procedure

This test was carried out with the sensor mounted in the test chamber shown in Figure 6a. For oxygen concentrations of 1%, 3%, 10%, and 20%, the sensor EMF was recorded at total pressures ranging from atmospheric (~14.7 psia) down to ~3 psia. The pressure was controlled by pumping on the test chamber with a mechanical vacuum pump through a throttling valve.

Because the metal can, shown in Figure 5b, is not rigid enough to withstand a large pressure difference without flexing, the thin film substrate was mounted on a rigid Forsterite ceramic plug for the purposes of this test. The sensor leads entered the test chamber through the ceramic material.

b.   Results

The results of this test are shown in Figure 27 and are tabulated in Table 22. Sensor No. 105Zr-7 was used at 181°C. At high oxygen pressures, the measured sensor EMF varies logarithmically with pressure in agreement with the predictions of the Nernst equation (Eq. 3). This is shown in the data for the 20% and 10% O_2 mixtures and for high total pressures with the 3% and 1% O_2 mixtures. At lower oxygen pressures, the EMF is slightly lower than predicted by the Nernst equation. This is exhibited by the low-total-pressure data for the 3% and 1% O_2 mixtures. This effect may occur because of the presence of hydrocarbons in the system due to backstreaming from the vacuum pump. The Phase 1 tests with C_3H_8 have shown that sensor EMF is depressed for small values of $P_{O_2}/P_{C_3H_8}$ and other hydrocarbons are expected to have a similar effect.

Figure 27 - Altitude
Simulation Test

ALTITUDE SIMULATION TEST
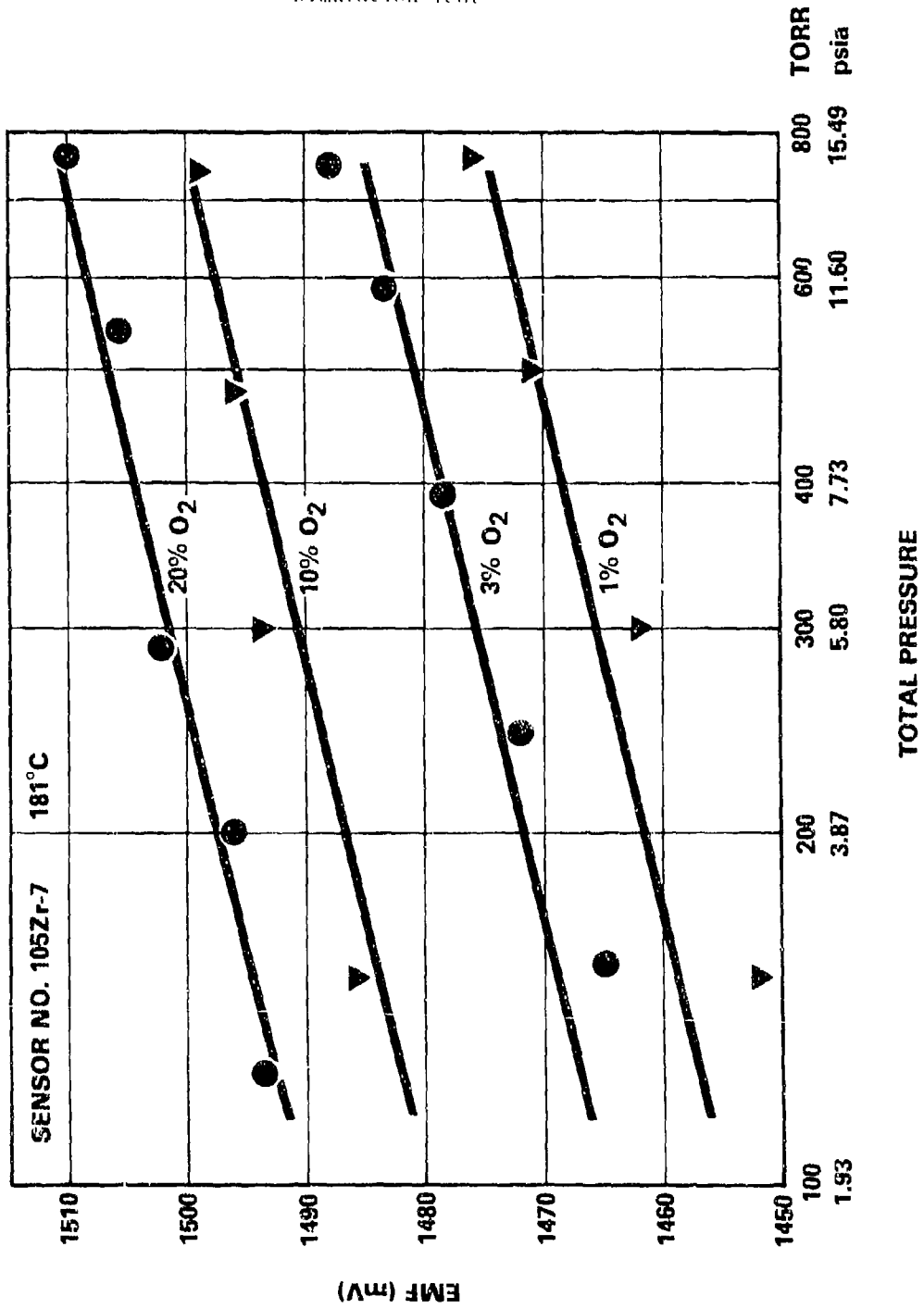
TABLE 22

ALTITUDE SIMULATION TEST

Sensor No. 105Zr-7 at 181°C

		P_{O_2} = 0.20 atm at 1 atm total pressure				
EMF (mV)	Measured	1510	1506	1502	1496	1493
	Nernstian		1507	1501	1497	1492
Total Pressure	(torr)	760	540	290	200	125
	(psia)	14.70	10.44	5.61	3.87	2.42

		P_{O_2} = 0.10 atm at 1 atm total pressure				
EMF (mV)	Measured	1499	1496	1494	1486	
	Nernstian		1495	1490	1483	
Total Pressure	(torr)	740	480	300	150	
	(psia)	14.31	9.28	5.80	2.90	

		P_{O_2} = 0.03 atm at 1 atm total pressure				
EMF (mV)	Measured	1488	1483	1479	1472	1465
	Nernstian		1486	1482	1477	1473
Total Pressure	(torr)	750	590	390	245	155
	(psia)	14.50	11.41	7.54	4.74	3.00

		P_{O_2} = 0.01 atm at 1 atm total pressure				
EMF (mV)	Measured	1476	1471	1462	1452	
	Nernstian		1472	1467	1460	
Total Pressure	(torr)	745	500	300	150	
	(psia)	14.41	9.67	5.80	2.90	

4. REDUCED TEMPERATURE TESTS

The effect on sensor performance of reducing the sensor temperature to a low value ($-30°C$) was measured. Such a temperature decrease could occur during system non-operation.

a. Experimental Procedure

The sensors for this test were mounted in the same way as those used for the altitude simulation test. Before cooling, the sensors were tested in O_2/N_2 atmospheres. They were then cooled from the operating temperature of $173°C$ to less than $-30°C$ in a period of one hour. The time-temperature profile is tabulated in Table 23. Temperatures below $-30°C$ were maintained for four hours. Cooling was achieved with crushed dry ice which was placed in the oven around the test chamber. After the required four hour cold period, the dry ice was allowed to sublime and the sensors and test chamber warmed to room temperature overnight. The sensors were then heated to the operating temperature and retested. During the cooldown, cold period, and warmup, the cyclic flow of O_2/N_2 mixtures through the test chamber was maintained. The cycle was 1% O_2 → 3% O_2 → 10% O_2 → 20% O_2 → 1% O_2 with each mixture flowing for 10 minutes.

b. Results

The EMF output of sensor 105Zr-9 for each of the four O_2 concentrations is listed before and after cooldown in Table 24. These data are the better of two sets of performance data obtained by testing sensors 105Zr-7 and 105Zr-9 simultaneously. Sensor 105Zr-9 had nearly identical sensing performance before and after exposure to reduced temperatures. The EMF levels for sensor 105Zr-7 were approximately 10 mV lower after cooling than before. However, based on the data listed in Table 24 it is clear that thin film oxygen sensors can withstand temperatures as low as $-55°C$ and thermal shocks in excess of $211°C/hr$ ($3.5°C/min$).

5. WATER VAPOR TESTS

These tests were conducted in order to determine the effects of humidity on sensor performance.

a. Experimental Procedure

Sensors for this test were mounted in test chambers like the one shown in Figure 6b. The test setup was the same as for standard O_2/N_2 atmosphere tests except that water vapor was mixed with the inflowing O_2/N_2 gas mixtures. To accomplish this a tee was placed just outside the oven in the inflowing gas line. The top of a rotameter was inserted into the tee and the bottom of the rotameter was connected to a steam generator (to be described below) via a copper tube. The rotameter and copper tube were heated to ~$140°C$ to prevent condensation of the H_2O before it was mixed with the O_2/N_2 gas.

TABLE 23

TIME TEMPERATURE PROFILE

Sensor No. 105Zr-9

Time After Start of Cooldown (min)	Temperature (°C)
0	173
5	141
10	116
15	97
20	80
25	68
30	59
35	52
40	40
45	13
50	-1
55	-28
60	-38
97	-52
162	-35
186	-55
210	-46
231	-37
256	-47
285	-56
300	-52

TABLE 24

REDUCED TEMPERATURE TEST

Sensor No. 10Zr-9 at 173°C

| P_{O_2} (atm) | Last Cycle Before Cooling | | After Reheating[a] | | Nernstian |
	EMF (mV)	ΔE (mV)	EMF (mV)	ΔE (mV)	ΔE (mV)
0.01	1269	0	1272	0	0
0.03	1282	13	1282	10	11
0.10	1300	31	1299	27	22
0.20	1310	41	1310	38	29

[a]These results are for the first complete cycle after
thermal equilibrium was established at 173°C. This
was the fourth cycle after the temperature reached
the neighborhood of 173°C. Each cycle lasted 40
minutes.

The steam generator consisted of a stainless steel heater and a sealed lid. The lid was provided with a pressure relief valve set at ~1 psig and a throttling valve for controlling the H_2O flow into the sensor test chambers. The generator was heated by a variable temperature electric hot plate.

The flow rate of the H_2O going into the test chambers was computed by using the rotameter reading, properly corrected for temperature and molecular weight. A rotameter was used, as usual, to determine the flow rate of the O_2/N_2 mixture. From the flow rate data, the relative humidity was computed.

With a 20% O_2 mixture flowing in the test chambers, the valve on the steam generator was opened and adjusted to give an H_2O flow equivalent to 40% and then 80% relative humidity at 21°C (70°F). EMF readings were recorded before opening the valve and at each relative humidity setting. Then the valve was closed and the sensor was allowed to return to equilibrium before the final EMF reading was recorded.

b.   Results

This test was run with three sensors simultaneously and was done at 143 and 168°C. Characteristic results are given in Table 25. The sensors respond to the introduction of water vapor by an increase in the sensor EMF as the humidity is increased from zero to ~40% (at 21°C). As the humidity is increased further to ~80% (at 21°C) the sensor EMF decreases and, in some cases, the decrease is to a value below the original EMF. The post-test sensor EMF was in all cases somewhat lower (~10 mV) than the pre-test sensor EMF. No further tests were conducted to determine if a continued decrease in the sensor EMF would result upon repeated exposure to high humidity environments.

An additional test was run to determine that these devices continue to sense changes in P_{O_2} in the presence of water vapor. The results of this test indicate that the changes in EMF are ~25% larger in the presence of water vapor than in dry O_2/N_2 mixtures.

Together, these tests indicate that the presence of water vapor affects but does not destroy the sensing characteristics of these devices.

6.   WATER VAPOR CONDENSATION TESTS

These tests were carried out to determine the effect of water vapor condensation forming on the sensors during system non-operation.

a.   Experimental Procedure

The same setup was used for this test as for the water vapor tests. With an 80% relative humidity (at 21°C) and 20% O_2 mixture flowing through the test chamber, the EMF was measured. The oven was turned off and the sensor assembly (see Figure 5b) cooled to a temperature just above the ice point. This caused condensation to form on the sensors. Then the oven was closed and turned on again. After the original temperature was reached, the EMF was recorded again.

69

TABLE 25

WATER VAPOR TESTS

Sensors in 0.2 atm O_2 Environment

Sensor No.	T (°C)	Pre-Test EMF (mV)	EMF With ~40% R.H.[a] (mV)	EMF With ~80% R.H.[b] (mV)	Post-Test EMF (mV)
105Zr-9	143	293	300	283	283
105Zr-11	168	958	990	986	948

[a]~40% relative humidity at 21°C (70°F).

[b]~80% relative humidity at 21°C (70°F).

b. Results

The results of tests on sensors 105Zr-6 and 105Zr-11 are shown in Table 26. The post-test EMF values were 60 mV and 195 mV lower, respectively, than the pre-test values. One hour elapsed after reaching thermal equilibrium before the post-test values were recorded. The EMF was, at that time, still increasing slowly (<10 mV/hr). It is possible that at least a part of the EMF difference is due to adsorbed H_2O remaining in the porous lead attachment medium.

7. TANK SEALANT TESTS

Sealant compounds are used to seal fuel tanks. Typically, a sensor in a fuel tank will be subjected to gases from these compounds. In order to simulate this condition, a small amount of a fuel tank sealant provided by AFAPL/SFH was placed in the gas stream such that outgassing from the sealant passed over the sensors. Cured and uncured sealant at room temperature and at the sensor operating temperature were used.

a. Experimental Procedure

Sensors were installed in chambers as shown in Figure 6b and tested with a cycle of O_2/N_2 mixtures. After a number of cycles, a 1/4 inch pipe plug in a tee in the gas stream was replaced with a second pipe plug having tank sealant on the face exposed to the gas stream. The sealant was Products Research and Chemical Corp. PR-1422, Class B-2. After a suitable number of additional gas cycles, the contaminated plug was replaced with the clean plug and several more gas cycles were completed. A tee outside the oven and another inside allowed for testing with the tank sealant at room temperature or at sensor operating temperature, respectively.

The tank sealant was applied to the pipe plug immediately before gas stream exposure for the uncured sealant tests. For the cured sealant tests, the sealant was applied and cured for seven days at $\sim74°F$ and $\sim50\%$ relative humidity. Specifically, the sealant was cured in a sealed dessicator containing $Ca(NO_3)_2 \cdot 4H_2O$ which is in equilibrium at 76°F and 51% relative humidity.

b. Results with Uncured Tank Sealant

The results of measurements on sensor No. 105Zr-3 at 170°C with uncured sealant are shown in Table 27. For the sealant at room temperature, there is no irreversible effect on sensor performance although the vapors do cause a decrease in the EMF during exposure. The data showed that the size of the effect continued to diminish during the course of the ~2 hour exposure time. This indicates that the rate of gas effluence from the uncured sealant at room temperature decreases measureably during the initial hours after preparation.

71

TABLE 26

WATER VAPOR CONDENSATION TESTS

172°C and ∿80% R.H.

Sensor No.	EMF Before Condensation (mV)	EMF After Condensation[a] (mV)
105Zr-6	820	760
105Zr-11	1152	957

[a]Values ∿1 hour after reaching 172°C. The EMF was still increasing slowly at that time.

TABLE 27

UNCURED TANK SEALANT TESTS

Sensor No. 10ᵃr-3 at 170°C

Tank Sealant at Room Temperature

P_{O_2} (atm)	Before Exposure EMF (mV)	Before Exposure ΔE (mV)	During Exposure EMF (mV)	During Exposure ΔE (mV)	After Exposure EMF (mV)	After Exposure ΔE (mV)	Nernstian ΔE (mV)
0.01	1032	0	1001	0	1033	0	0
0.03	1041	9	1023	22	1043	10	11
0.10	1057	25	1046	45	1058	25	22
0.20	1068	36	1059	58	1069	36	29

Tank Sealant at Sensor Temperature

P_{O_2} (atm)	Before Exposure EMF (mV)	Before Exposure ΔE (mV)	During Exposure[a] EMF (mV)	During Exposure[a] ΔE (mV)	After Exposure EMF (mV)	After Exposure ΔE (mV)	Nernstian ΔE (mV)
0.01	1022	0	992	0	1008	0	0
0.03	1032	10	1009	17	1018	10	11
0.10	1047	25	1026	34	1034	26	22
0.20	1058	36	1038	46	1045	37	29

[a] Second cycle after inserting sealant into oven

[b] Sixth cycle after removing sealant.

The uncured sealant at the sensor temperature produces a very strong decrease in EMF when first introduced into the gas stream and heated. A new batch of sealant was mixed for this test so that it was less than 30 minutes old when used. The decrease in sensor EMF during the first few minutes was >100 mV as the sealant heavily outgassed. Within ten minutes, the response had returned to within 50 mV of the original EMF and after one 40 minute gas cycle, the data in Table 27 were taken. The continued decrease in gas effluence was obvious as long as the sealant remained in the gas stream. Upon removal of the sealant, the EMF responses returned to within 14 mV of the pre-test values and the ΔE values were within 1 mV of the pre-test values.

c. Results with Cured Tank Sealant

The results of measurements on sensor No. 105Zr-2 at 174°C with cured tank sealant are shown in Table 28. The sealant, at room temperature, causes no significant effect (≤ 2 mV) on the EMF. After removing the cured sealant from the gas stream a change of 3-8 mV was noted. The reason for this latter change is unclear.

With the cured sealant at the sensor temperature, the sensor response was similar to the response with the uncured sealant. That is, a large initial response falls off rapidly to a much smaller response. The "During Exposure" and "After Exposure" data shown in the table are for the first complete cycles following insertion of the sealant and following removal of the sealant, respectively.

8. RESPONSE OF SENSORS DELIVERED TO AFAPL/SFH

Five sensors of the best type developed under this program were tested after the conclusion of all other testing to assure proper functioning and were delivered to AFAPL/SFH. All five sensors are assembled from oxide films deposited from the 8 mole % Y_2O_3-92 mole % ZrO_2 sputtering target during sputter deposition run 105 (see Table 6). Each sensor uses one of three dc sputter deposited Pt electrodes. The substrate leads are Cu and the sensing electrode leads are Au except for sensor No. 105Zr-10 which has Pt wire leads. Lead attachment is accomplished with Au and/or Pt applied as colloids.

The final performance of each sensor is tabulated in Table 29 and a brief chronological record of each sensor is given below.

- 105Zr-1   Heat treated at 400°C for 15 minutes and at 450°C for 15 minutes. Electrodes applied, assembled, and tested for delivery to AFAPL/SFH.

- 105Zr-3   Heat treated at 400°C for 15 minutes and at 450°C for 15 minutes. Electrodes applied, assembled, and tested. Used for a reduced temperature test, uncured tank sealant tests, and soaked in JP-4 for 24 hours. Tested for delivery to AFAPL/SFH.

74

TABLE 28

CURED TANK SEALANT TESTS

Sensor No. 105Zr-2 at 174°C

Tank Sealant at Room Temperature

P_{O_2} (atm)	Before Exposure		During Exposure		After Exposure		Nernstian
	EMF (mV)	ΔE (mV)	EMF (mV)	ΔE (mV)	EMF (mV)	ΔE (mV)	ΔE (mV)
0.01	775	0	777	0	783	0	0
0.03	789	14	790	13	794	11	11
0.10	801	26	802	25	805	22	22
0.20	811	36	812	35	814	31	29

Tank Sealant at Sensor Temperature

P_{O_2} (atm)	Before Exposure		During Exposure		After Exposure		Nernstian
	EMF (mV)	ΔE (mV)	EMF (mV)	ΔE (mV)	EMF (mV)	ΔE (mV)	ΔE (mV)
0.01	736	0	768	0	788	0	0
0.03	796	10	783	15	798	10	11
0.10	807	21	799	31	812	24	22
0.20	816	30	808	40	820	32	29

- 105Zr-7   Heat treated at 450°C for 15 minutes. Electrodes applied, assembled, and tested. Used for altitude tests and a reduced temperature test. Tested for delivery to AFAPL/SFH.

- 105Zr-9   Heat treated at 450°C for 15 minutes. Electrodes applied, assembled, and tested, Used for altitude tests, a reduced temperature test, a water vapor test, and a water vapor condensation test. Tested for delivery to AFAPL/SFH.

-105Zr-10   Heat treated at 450°C for 15 minutes. Electrodes applied, assembled, and tested. Used for test to determine the effect of JP-4 dropping onto an operating sensor. Tested for delivery to AFAPL/SFH.

9. REPRODUCIBILITY

The data reported in this section are all for samples from the same sputter deposition run and, in many cases, several data for the same sensor are reported. There is a substantial variation in the EMF values which points to the need for an end to the use of the laboratory methods used for sensor fabrication, especially the lead attachment techniques. The laboratory procedures should be replaced by industrial microcircuit procedures for substrate preparation, electrolyte film deposition, lead attachment, and sensor package assembly. The variation in EMF values which have been observed are almost certainly due to unavoidable variations in substrate cleaning and lead attachments, both of which have been done by hand. It is imperative that precisely controlled, reproducible microcircuit manufacturing methods be used for the further development of this type of sensor.

TABLE 29

RESPONSE OF SENSORS DELIVERED TO AFAPL/SFH

Sensor No.	T (°C)	Sensor EMF (mV) and ΔE (mV) at P_{O_2} (atm) indicated							
		EMF at 0.01	ΔE	EMF at 0.03	ΔE	EMF at 0.10	ΔE	EMF at 0.20	ΔE
105Zr-1	177	1172	0	1182	10	1189	17	1197	25
105Zr-3	177	1035	0	1049	14	1062	27	1073	38
105Zr-7	173	1129	0	1141	12	1149	20	1161	32
105Zr-9	173	1216	0	1230	14	1237	21	1250	34
105Zr-10	176	884	0	902	18	913	29	932	48
Nernstian	176		0		11		22		29

SECTION VI

CONCLUSIONS AND RECOMMENDATIONS

1. PHASE I CONCLUSIONS

As demonstrated by the Phase I results presented in Section IV of this report, major improvements have been made in the performance and reliability of oxygen sensing devices using a thin solid electrolyte film. The overall accomplishments of Phase I of this program can be stated as follows:

   a. A large number of sensors have been prepared using a number of different deposition conditions for both the thin solid electrolyte films and the electrodes.

   b. Oxygen sensing devices have been characterized as to their physical properties and sensing performance in various O_2/N_2 mixtures to determine both the optimum deposition conditions and the sensing performance which are attainable with thin solid electrolyte film devices.

   c. The effect of various contaminant gases on sensing performance has been determined.

The conclusions derived from Phase I of this program are briefly summarized below.

   a. Solid Electrolyte Films

The quality of Y_2O_3 doped ZrO_2 films prepared by rf sputter deposition depends on deposition parameters, particularly the applied substrate bias. The highest quality films during Phase I have been prepared with an applied substrate bias of ~-80 V at a target voltage of -500 V and with an applied substrate bias of ~-50 V at a target voltage of -300 V. Analysis of these films by sophisticated analytical techniques indicates these films are slightly oxygen deficient but have a homogeneous morphology. The sensing performance of these films is improved if a high temperature heat treatment is used to reduce the oxygen deficiency of the films prior to device assembly.

   b. Electrode Optimization

A survey of electrode types demonstrated that the best sensing performance was obtained with sputter deposited platinum electrodes about 50 nm thick.

   c. Device Oxygen Sensing Performance

Sensing performance of a number of devices was determined from 90 to 200°C. Oxygen sensing was obtained over this temperature range with a response time, for an increase in the oxygen partial pressure, of less than one minute at 150°C for a typical sensor. In devices

78

where the solid electrolyte has been heated in air prior to device assembly, actual EMF output of the device is very close to the predicted EMF output.

d. Effect of Contaminant Gases on Sensor Performance

The presence of H_2O vapor, CO_2, SO_2, NO_2, or C_3H_8 at contractually required concentrations alters the performance of this type of device by shifting the voltage output. In the case of H_2O vapor, CO_2, and SO_2, this effect is small. For NO_2 and C_3H_8 the voltage shift is large. In no case is the sensing performance destroyed by exposure to these contaminants. Additional tests performed with the C_3H_8 gas contaminant, which caused the largest voltage shift, indicated that the oxygen sensing performance of these devices is _enhanced_ by the presence of C_3H_8.

2. PHASE II CONCLUSIONS

The results of Phase II of this program demonstrate that the oxygen sensing devices developed during Phase I can be expected to operate in an aircraft fuel tank ullage space if the method of installation prevents repeated sloshing of liquid fuel onto the sensor. In fact, lead detachment was the only mechanism by which sensing devices actually failed and this problem would not be encountered in a device assembled by commercial microcircuit techniques. Spurious results may have occurred in some of the tests reported in Sections IV and V as a result of partial lead detachment or contaminant adsorption on the porous lead attachment material. Nonetheless, the following minimum conclusions can be made regarding the performance to be expected of this type of oxygen sensor operating in an aircraft fuel tank environment.

- Short term exposure of operating or non-operating sensors to liquid fuel has no deleterious effect on the sensor EMF output. Repeated fuel contact may cause an increase in sensor response time.

- The variation of sensor output at simulated altitudes varies in agreement with theory and can be compensated electronically.

- Reduced temperatures (to -30°C) during device non-operation have negligible effect on sensor performance.

- Although sensing performance was modified, the sensors continued to operate in the presence of water vapor (humidity).

- Condensation of water onto the sensors alters the oxygen sensing performance but does not destroy the sensors.

- Tank sealant vapors depressed sensor output during sealant curing. Relatively smaller alterations in sensor performance were noted with nearly cured tank sealant. For all sensors, oxygen sensing continued in the presence of sealant vapors.

3. RECOMMENDATIONS

The results of this program indicate that oxygen sensing devices of this type show sufficient promise of becoming operational that their development should be continued. At this point it is recommended that the thin electrolyte film production and the integration of the films into sensor assemblies can best be carried out with the techniques and facilities used for commercial microcircuit production. In order to bring the development of this type of sensor to the prototype stage, it is recommended that the following steps be taken:

- Design and construct more rugged sensors which are capable of being flight tested using standard microcircuit techniques.

- Determine the reproducibility of oxygen sensing performance both within each production batch and between batches.

- Determine the long term stability of oxygen sensing performance.

- Establish performance tests which more closely simulate fuel tank conditions than those carried out during Phase II of this program.

- Flight test a prototype sensor if the above steps are completed successfully.

It is believed that these recommendations can be carried out in a straight-forward manner and that the likelihood of success is great enough to merit carrying on the development of this type of sensor.

THIS REPORT HAS BEEN DELIMITED
AND CLEARED FOR PUBLIC RELEASE
UNDER DOD DIRECTIVE 5200.20 AND
NO RESTRICTIONS ARE IMPOSED UPON
ITS USE AND DISCLOSURE.

DISTRIBUTION STATEMENT A

APPROVED FOR PUBLIC RELEASE;
DISTRIBUTION UNLIMITED.